Научном већу Института за физику у Београду

Београд, 28. октобар 2024. године

Предмет: Молба за покретање поступка за реизбор у звање
научни сарадник

М О Л Б А

С обзиром да испуњавам критеријуме прописане од стране Министарства науке, технолошког развоја и иновација Републике Србије за звање научни сарадник, молим Научно веће Института за физику у Београду да покрене поступак за мој реизбор у наведено звање.

У прилогу достављам:

1. мишљење руководиоца лабораторије са предлогом чланова комисије за реизбор у наведено звање;

2. стручну биографију;

3. преглед научне активности;

4. елементе за квалитативну и квантитативну оцену научног доприноса са доказима;

5. списак и копије објављених радова и других публикација;

6. податке о цитираности;

7. копију решења о претходном избору у звање;

8. додатне прилоге који документују наводе.

С поштовањем,

др Душан Вудраговић

Научном већу Института за физику у Београду

Предмет: Мишљење руководиоца Центра о реизбору др Душана Вудраговића у звање научни сарадник

Др Душан Вудраговић је запослен у Лабораторији за примену рачунара у науци, у оквиру Националног центра изузетних вредности за изучавање комплексних система Института за физику у Београду. У истраживачком раду бави се физиком ултрахладних диполних Бозе гасова, као и развојем паралелних нумеричких алгоритама за проучавање оваквих система. С обзиром да испуњава све предвиђене услове у складу са Правилником о стицању истраживачких и научних звања, сагласан сам са покретањем поступка за избор др Душана Вудраговића у звање научни сарадник.

За састав комисије за реизбор др Душана Вудраговића у звање научни сарадник предлажем:

(1) др Антун Балаж, научни саветник, Институт за физику у Београду,
(2) др Ивана Васић, виши научни сарадник, Институт за физику у Београду,
(3) академик Милан Дамњановић, професор емеритус Универзитета у Београду.

др Антун Балаж
научни саветник
руководилац Центра за изучавање
комплексних система

Стручна биографија Душана Вудраговића

Душан Вудраговић је рођен 3. маја 1980. године у Сремској Митровици. Основну школу Доситеј Обрадовић завршио је у Путинцима, а Гимназију Стеван Пузић у Руми. Основне студије је похађао на Физичком факултету Универзитета у Београду на смеру Примењена физика и информатика у периоду од 1999. до 2005. године. Током студија добио је стипендије Министарства науке Републике Србије и Владе Републике Србије, као и награду 1000 најбољих студената у Србији Норвешке амбасаде у Београду. Дипломирао је 2005. године са просечном оценом 9.62. Дипломски рад под називом Мерење ефективне трансверзалне емитансе јонског снопа урадио је под руководством проф. др Ивана Аничина.

У периоду од 2006. до 2008. године боравио је у ЦЕРН-у (Женева) као сарадник на FP6 пројектима SEE-GRID-2 (SEE-GRID eInfrastructure for regional eScience) и EGEE-II (Enabling Grids for E-sciencE).

Докторске студије на Физичком факултету Универзитета у Београду уписао је 2012. године. Докторску дисертацију под насловом Faraday waves in ultracold dipolar Bose gases (Фарадејеви таласи у ултрахладним диполним Бозе гасовима) урађену под менторством др Антуна Балажа, одбранио је 24. децембра 2019. године.

Душан Вудраговић је запослен у Институту за физику у Београду као научни сарадник у Лабораторији за примену рачунара у науци Националног центра изузетних вредности за изучавање комплексних система. Тренутно учествује у реализацији пројекта CTRUST (Topology-derived methods for the analysis of collective trust dynamics) Фонда за науку Републике Србије. У оквиру међународне сарадње, тренутно је ангажован на Хоризонт пројектима Skills4EOSC (Skills for the European Open Science commons: creating a training ecosystem for Open and FAIR science) и EOSC Beyond (EOSC Beyond: advancing innovation and collaboration for research), као и на пројекту EuroCC2 (National Competence Centres in the framework of EuroHPC) из програма Digital Europe.

Душан Вудраговић је делегат Института за физику у Београду у генералној скупштини EOSC (European Open Science Cloud) асоцијације. У оквиру ове организације активно учествује у раду радне групе за техничку и семантичку интероперабилност EOSC-а која има за циљ да омогући једноставан приступ истраживачким ресурсима и резултатима широм Европе.

До сада је Душан Вудраговић објавио 25 радова у међународним часописима и више саопштења са међународних скупова штампаних у изводу.

Преглед научне активности Душана Вудраговића

Душан Вудраговић ради у Лабораторији за примену рачунара у науци на Институту за физику у Београду. У свом научном раду бави се проблемима ултрахладних бозонских гасова у присуству дипол-дипол интеракције, као и развојем паралелних нумеричких алгоритама и програма за нумеричке симулације ових физичких система.

Кандидат је успешно развио и имплементирао нумерички метод подељеног корака за решавање Грос-Питаевски једначине са контактним и диполним интеракционим чланом. Метод је прво развијен за ултрахладне Бозе гасове чије се интеракције могу описати помоћу контактног интеракционог потенцијала, а затим је уопштен на системе у којима се, поред контактне, у обзир мора узети и дипол-дипол интеракција. Развијени метод омогућава разматрање анизотропних тродимензионалних система, али је проширен и на специјалне ниже-димензионалне случајеве који узимају у обзир различите симетрије замке у којој је смештен Бозе-Ајнштајн кондензат: тродимензионалне аксијално- и радијално-симетричне замке, дводимензионалне цилиндрично-симетричне замке, изотропне сферно-симетричне и анизотропне једнодимезионалне и дводимензионалне замке. Рачунарски кодови су паралелизовани и прилагођени за коришћење на графичким картицама. Резултати су представљени у следећим међународним часописима:

- **D. Vudragović**, I. Vidanović, A. Balaž, P. Muruganandam, and S. K. Adhikari, *C Programs for Solving the Time-dependent Gross-Pitaevskii Equation in a Fully Anisotropic Trap*, Comput. Phys. Commun. **183**, 2021 (2012),
  M21a; DOI: 10.1016/j.cpc.2009.04.015; IF(2012) = 3.078;

- R. Kishor Kumar, L. Young-S., **D. Vudragović**, A. Balaž, P. Muruganandam, and S. K. Adhikari, *Fortran and C Programs for the Time-dependent Dipolar Gross-Pitaevskii Equation in an Anisotropic Trap*, Comput. Phys. Commun. **195**, 117 (2015),
  M21a; DOI: 10.1016/j.cpc.2015.03.024; IF(2015) = 3.635;

- L. Young-S., **D. Vudragović**, P. Muruganandam, S. K. Adhikari, and A. Balaž, *OpenMP Fortran and C Programs for Solving the Time-dependent Gross-Pitaevskii Equation in an Anisotropic Trap*, Comput. Phys. Commun. **204**, 209 (2016),
  M21a; DOI: 10.1016/j.cpc.2016.03.015; IF(2016) = 3.936;

- L. Young-S., P. Muruganandam, S. K. Adhikari, V. Loncar, **D. Vudragović**, and A. Balaž, *OpenMP GNU and Intel Fortran programs for solving the time-dependent Gross-Pitaevskii equation*, Comput. Phys. Commun. **220**, 503 (2017),
  M21a; DOI: 10.1016/j.cpc.2017.07.013; IF(2017) = 3.748.

- R. Ravisankar, **D. Vudragović**, P. Muruganandam, A. Balaž, and S. K. Adhikari, *Spin-1 Spin-orbit- and Rabi-coupled Bose-Einstein Condensate Solver*, Comput. Phys. Commun. **259**, 107657 (2021),
  M21a; DOI: 10.1016/j.cpc.2020.107657; IF(2021) = 4.717.

У свом истраживању Душан Вудраговић је проучавао феномене Фарадејевих и ре-

зонантних таласа густине у ултрахладним бозонским системима са контактном и дипол-дипол интеракцијом. Овакви таласи настају као резултат хармонијске модулације система и представљају нелинеарне ексцитације система услед присуства интеракција, спрезањем колективних осцилација и параметарских резонанци. У оквиру теорије средњег поља развио је варијациони приступ за опис динамике Фарадејевих и резонантних таласа у диполним кондензатима. Овај приступ је заснован на Гаусовом варијационом анзацу који за параметре има ширине кондензата, коњуговане фазе, а укључује и модулације густине како би описао динамику таласа густине.

Користећи развијени варијациони приступ, као и пун нумерички приступ, детаљно је проучавао особине таласа густине у диполним кондензатима на нултој температури, где дипол-дипол интеракција игра важну улогу због нарушења симетрије услед анизотропије система. Извео је једначине кретања које описују динамику модулисаног диполног бозонског система и идентификовао најнестабилније моде које одговарају Фарадејевим и резонантним таласима. Даље, на основу тога, извео је аналитичке изразе за просторне периоде оба типа таласа густине, као и њихову зависност од јачине контактне и дипол-дипол интеракције. Добијене варијационе резултате упоредио је са резултатима детаљних нумеричких симулација које решавају диполну Грос-Питаевски једначину у три просторне димензије и добио веома добро слагање.

Душан Вудраговић је проучавао и утицај контактне и дипол-дипол интеракције на својства основног стања и колективних осцилација диполних кондензата. Док повећање јачине контактне интеракције увек доводи до ширења кондензата, ситуација је сложенија када се мења јачина дипол-дипол интеракције. За замку у облику цигаре у којој су диполи оријентисани у радијалном смеру, показао је да повећање јачине дипол-дипол интеракције доводи до ширења кондензата у лонгитудиналном правцу и у правцу поларизације, док се ширина у трећем правцу смањује. Поред тога, проучавао је и фреквенције колективних мода, где су ефекти интеракција мање изражени. Ово се посебно односи на монополну (дишућу) и квадруполну моду, чије вредности практично остају константне у целом распону експериментално релевантних вредности јачина интеракција. Са друге стране, фреквенција радијалне квадруполне моде је осетљивија на промену јачине интеракције, посебно јачине контактне интеракције, док при промени јачине дипол-дипол интеракције показује немонотоно понашање. Резултати су представљени у следећем међународном часопису:

- **D. Vudragović** and A. Balaž, *Faraday and Resonant Waves in Dipolar Cigar-Shaped Bose-Einstein Condensates*, Symmetry **11**, 1090 (2019), M22; DOI: 10.3390/sym11091090; IF(2019) = 2.645.

Елементи за квалитативну оцену научног доприноса Душана Вудраговића

1 Квалитет научних резултата

1.1 Значај научних резултата

Најзначајнији радови др Душана Вудраговића су:

- **D. Vudragović** and A. Balaž, *Faraday and Resonant Waves in Dipolar Cigar-Shaped Bose-Einstein Condensates*, Symmetry **11**, 1090 (2019)
  M22; DOI: 10.3390/sym11091090; IF(2019) = 2.645;

- **D. Vudragović**, I. Vidanović, A. Balaž, P. Muruganandam, and S. K. Adhikari, *C Programs for Solving the Time-dependent Gross-Pitaevskii Equation in a Fully Anisotropic Trap*, Comput. Phys. Commun. **183**, 2021 (2012)
  M21a; DOI: 10.1016/j.cpc.2009.04.015; IF(2012) = 3.078.

У првом раду кандидат је развио варијациони и нумерички приступ за проучавање особина таласа густине у диполним кондензатима на нултој температури, где дипол-дипол интеракција игра важну улогу због нарушења симетрије услед анизотропије система. Користећи ове приступе, проучио је:

- колективне осцилације и динамику Фарадејевих таласа у ултрахладним бозонским системима са контактном и дипол-дипол интеракцијом;

- појаву резонантних таласа и утицај дипол-дипол интеракције на њихове особине у диполним Бозе-Ајнштајн-кондензованим системима.

Утицај контактне и дипол-дипол интеракције на фреквенције колективних мода и особине Фарадејевих таласа у диполним Бозе-Ајнштајн кондензатима испитао је детаљним нумеричким симулацијама и варијационим приступом. Посебно је проучавао зависност просторног и временског периода Фарадејевих таласа од јачине дипол-дипол интеракције. Сви прорачуни су изведени за реалистичне физичке системе, као што су атомски гасови хрома, диспрозијума и ербијума.

Типично време развоја резонантних таласа је много мање од времена које је потребно за појаву Фарадејевих таласа. Кандидат је проучио утицај јачине диполне интеракције на ова карактеристична времена. Такође, испитао је раније уочени феномен појаве снажнијег резонантног одговора система за модулациону фреквенцију која је двоструко већа од радијалне фреквенције замке, иако би се очекивало да се најважнија резонанца добија када су ове фреквенције једнаке.

У другом раду кандидат је развио нумеричку методу за решавање Грос-Питаевски једначине за ултрахладне бозонске системе са диполном интеракцијом, која представља резултат теорије средњег поља. Временски зависна диполна Грос-Питаевски једначина је парцијална диференцијална једначина по просторним координатама и времену и има структуру нелинеарне Шредингерове једначине, тако да садржи први извод таласне функције по времену и друге изводе по просторним координатама. Ди-

полни интеракциони члан је описан помоћу просторног интеграла, пошто је у питању дугодоментна интеракција. Развијени метод подељеног корака за решавање Грос-Питаевски једначине укључује дискретизацију по простору и времену, појединачну интеграцију по просторним координатама и временску пропагацију дискретизоване једначине. С обзиром на велику нумеричку захтевност тродимензионалних симулација за проучавање реалних физичких система, сви алгоритми су паралелизовани и прилагођени за коришћење на графичким картицама.

1.2 Параметри квалитета часописа

Кандидат др Душан Вудраговић је објавио укупно 9 радова у међународним часописима и то:

- 5 радова у међународним часописима изузетних вредности *Computer Physics Communications* следећих импакт фактора IF(2021) = 4.717, IF(2017) = 3.748, IF(2016) = 3.936, IF(2015) = 3.635, IF(2012) = 3.078, односно SNIP(2021) = 2.271, SNIP(2017) = 1.909, SNIP(2016) = 1.961, SNIP(2015) = 1.869, SNIP(2012) = 2.102.

- 3 рада у врхунским међународним часописима *Journal of Grid Computing, Communications in Computational Physics* и *Nuclear Instruments and Methods in Physics Research Section B* следећих импакт фактора IF(2011) = 1.310, IF(2012) = 1.863, IF(2015) = 1.389, односно SNIP(2011) = 1.902, SNIP(2012) = 1.320, SNIP(2015) = 1.003, redom;

- 1 рад у истакнутом међународном часопису *Symmetry* импакт фактора IF(2019) = 2.645, односно SNIP(2018) = 1.028.

Библиометријски показатељи су сумирани у следећој табели.

	IF	**M**	**SNIP**
Укупно	26.321	79.0	15.365
Усредњено по чланку	2.925	8.8	1.707
Усредњено по аутору	5.514	15.0	2.946

1.3 Позитивна цитираност научних радова

Према подацима из базе Web of Science, радови Душана Вудраговића цитирани су укупно 402 пута, од чега 393 пута изузимајући аутоцитате. Хиршов индекс је 7.

1.4 Међународна сарадња

Кандидат има изражену међународну сарадњу. Активно сарађује са групама др Садхана Кумара Адхикарија са Државног универзитета у Сао Паулу (Бразил), др Александру Николина са Универзитета у Букурешту (Румунија) и др Аксела Пелстера са Техничког универзитета у Кајзерслаутерну (Немачка). Поред тога, др Душан Вудраговић је учествовао на 3 билатерална пројекта између Србије и Немачке и на 18 пројеката Европске комисије у програмима FP6, FP7, Horizon 2020, Horizon Europe и Digital Europe. На већини ових пројеката био је руководилац радних пакета или радних задатака.

2 Нормирање броја коауторских радова, патената и техничких решења

Окосница свих радова кандидата је развој нумеричких метода за проучавање особина диполних кондензата у којима дипол-дипол интеракција игра важну улогу због нарушења симетрије услед анизотропије система. Радови кандидата категорије М21а имају 5 или 6 аутора, па ови радови не мењају значајно нормиран број бодова.

3 Учешће у пројектима, потпројектима и пројектним задацима

Кандидат је учествовао на следећим националним пројектима:

- CTRUST (2024-2026) - Topology-derived methods for the analysis of collective trust dynamics, Фонд за науку Републике Србије, Програм ПРИЗМА;

- ATLAS (2020-2022) - Artificial Intelligence Theoretical Foundations for Advanced Spatio-Temporal Modelling of Data and Processes, Фонд за науку Републике Србије, Програм за развој пројеката из области вештачке интелигенције;

- пројекат Министарства просвете, науке и технолошког развоја Републике Србије ОН171017 Моделирање и нумеричке симулације сложених вишечестичних система;

- пројекат Министарства просвете, науке и технолошког развоја Републике Србије ИИИ43007 Истраживање климатских промена и њиховог утицаја на животну средину - праћење утицаја, адаптација и ублажавање.

Кандидат је учествовао на билатералним пројектима Србије и Немачке (QDDB, IBEC, BEC-L) у периоду од 2013. до 2020. године.

Кандидат је учествовао на следећим међународним пројектима као руководилац радног пакета:

- EuroCC2 (2023-2025), National Competence Centres in the framework of EuroHPC; European Commission, Digital Europe programme;

- NI4OS-Europe (2019-2022), National Initiatives for Open Science in Europe; European Commission, Horizon 2020, Implementing the European Open Science Cloud;

- VI-SEEM (2015-2018), Virtual Research Environment (VRE) in Southeast Europe and the Eastern Mediterranean (SEEM); European Commission, Horizon 2020, Research and innovation programme;

- SemaGrow (2012-2015), Data intensive techniques to boost the real-time performance of global agricultural data infrastructures; European Commission, FP7, Research infrastructures project;

- agINFRA (2011-2014), A data infrastructure to support agricultural scientific communities Promoting data sharing and development of trust in agricultural sciences; European Commission, FP7, Research infrastructures project;

- HP-SEE (2010-2012), High-Performance Computing Infrastructure for South East Europe's Research Communities; European Commission, FP7, Research infrastructures project.

Кандидат је учествовао на следећим међународним пројектима као руководилац радног задатка:

- EOSC Beyond (2024-2027), EOSC Beyond: Advancing innovation and collaboration for research; European Commission, Horizon Europe programme;

- SMARTCHAIN (2018-2021), Towards Innovation - driven and smart solutions in short food supply chains; European Commission, Horizon 2020, Research and innovation programme;

- SEE-GRID-SCI (2008-2010), European Commission, FP7 project;

- LA@CERN (2008-2010), European Commission, Lifelong Learning Programme.

Кандидат је учествовао на следећим међународним пројектима као члан пројектог тима:

- Skills4EOSC (2022-2025), Skills for the European Open Science commons: creating a training ecosystem for Open and FAIR science; European Commission, Horizon Europe programme;

- PRACE-3IP (2012-2014), Partnership for Advanced Computing in Europe - Third Implementation Phase Project; European Commission, FP7, Research infrastructures project;

- PRACE-2IP (2011-2013), Partnership for Advanced Computing in Europe AISBL - Second Implementation Phase Project; European Commission, FP7, Research infrastructures project;

- PRACE-1IP (2010-2012), Partnership for Advanced Computing in Europe AISBL - First Implementation Phase Project; European Commission, FP7, Research infrastructures project;

- EGI-InSPIRE (2010-2014), Integrated Sustainable Pan-European Infrastructure for Researchers in Europe; European Commission, FP7, Research infrastructures project;

- EGEE-III (2008-2010), European Commission, FP7 project;

- EGEE-II (2006-2008), Enabling Grids for E-sciencE; European Commission, FP6, eInfrastructure project;

- SEE-GRID-2 (2006-2008), South Eastern European Grid-enabled eInfrastructure Development; European Commission, FP-6, regional eInfrastructure project.

4 Активност у научним и научно-стручним друштвима

4.1 Рецензије научних радова

Др Душан Вудраговић је био рецензент:

- 5 радова у часопису Data Technologies and Applications;

- 2 рада у часопису Physics Letters A;

- 2 рада у часопису Applied Physics B;

- 1 рада у часопису Simulation: Journal of Physics: Condensed Matter;

- 1 рада у часопису Simulation: Transactions of the Society for Modeling and Simulation International.

4.2   Организација научних скупова

Др Душан Вудраговић био је члан организационог одбора следећих конференција:

- EOSC Regional Event by NI4OS-Europe која је одржана од 28. до 29. septembra 2022. године на Универзитету технологије и економије, Будимпешта, Мађарска.

- HP-SEE User Forum 2012, која је одржана од 17. до 19. октобра 2012. године у Народној библиотеци Србије у Београду.

4.3   Педагошки рад

Др Душан Вудраговић је организовао више уводних и напредних High-performance i High-throughput компјутинг регионалних тренинга који су у просеку трајали два дана и на којима је у просеку по тренингу учествовало 30 људи. Овде су наведени само неки од њих:

- Machine Learning for Multiple Domains: From Concepts to Implementation, 14-15 October 2024, Online;

- High performance computing in function of business enhancement, 14-15 June 2018, Belgrade, Serbia;

- VI-SEEM regional climate training event, 11-13 October 2017, Belgrade, Serbia;

- VI-SEEM life sciences regional training, 19-21 October 2016, Belgrade, Serbia;

У периоду од 2015. до 2016. године објавио је серију чланака под називом Природа кода у часопису Млади физичар, а од 2014. године учествује као предавач на Научно-едукативном кампу Михајло Идворски Пупин у Идвору.

5   Утицај научних резултата

Утицај научних резултата се огледа у броју цитата који су наведени у тачки 1.3. овог одељка, а значај резултата је описан у тачки 1. Овде се може навести и чињеница да је један M21a рад, на ком је кандидат први аутор, високо цитиран (тренутни број цитата је 186) и да је омогућио објављивање низа других публикација.

6 Конкретан допринос кандидата у реализацији радова у научним центрима у земљи и иностранству

Кандидат је све своје истраживачке активности реализовао у Институту за физику у Београду. Кандидат је дао кључни допринос у свим објављеним радовима, а његов допринос се огледа у изради потребних нумеричких симулација, добијању, интерпретацији и презентацији нумеричких резултата, писању радова и комуникацији са уредницима и рецензентима часописа.

Елементи за квантитативну оцену научног доприноса Душана Вудраговића

7 Остварени М-бодови по категоријама публикација

Категорија	М-бодова по публикацији	Број публикација	Укупно М-бодова (нормирано)
М13	7.0	1	7.0 (5.0)
М21а	10.0	1	10.0 (10.0)
М34	0.5	5	2.5 (2.0)

8 Поређење оствареног броја М-бодова са минималним условима потребним за избор у звање научног сарадника

	Потребно	Остварено (нормирано)
Укупно	16.0	19.5 (17.0)
М10+М20+М31+М32+М33+М41+М42	10.0	17.0 (15.0)
М11+М12+М21+М22+М23	6.0	10.0 (10.0)

Списак објављених радова и других публикација који се бодују

Монографска студија/поглавље у књизи М11 или рад у тематском зборнику водећег међународног значаја (М13)

1. S. Stanišić, M. Perišić, G. Jovanović, D. Maletić, **D. Vudragović**, A. Vranić, and A. Stojić, *What Information on Volatile Organic Compounds Can Be Obtained from the Data of a Single Measurement Site Through the Use of Artificial Intelligence?*, Artificial Intelligence: Theory and Applications, Ed. Endre Pap, p. 207-225, Springer (2021),
DOI: 10.1007/978-3-030-72711-6_12.

Радови у међународним часописима изузетних вредности (М21а)

1. R. Ravisankar, **D. Vudragović**, P. Muruganandam, A. Balaž, and S. K. Adhikari, *Spin-1 Spin-orbit- and Rabi-coupled Bose-Einstein Condensate Solver*, Comput. Phys. Commun. **259**, 107657 (2021),
DOI: 10.1016/j.cpc.2020.107657; IF(2021) = 4.717.

Саопштења са међународних скупова штампана у изводу (М34)

1. **D. Vudragović**, *Faraday and Resonant Waves in Dipolar Cigar-Shaped Bose-Einstein Condensates*, The 8th International School and Conference on Photonics, Belgrade, Serbia, 23-27 August 2021.

2. M. Perišić, A. Stojić, G. Jovanović, A. Šoštarić, D. Maletić, **D. Vudragović**, and S. Stanišić, *The potential for forecasting the particulate matter levels in complex urban environment*, International Conference of Experimental and Numerical Investigations and New Technologies, Zlatibor, Serbia, 29 Jun–2 July 2021.

3. S. Stanišić, M. Perišić, A. Stojić, A. Šoštarić, **D. Vudragović**, D. Maletić, and G. Jovanović, *The impact of gaseous pollutants on particulate matter distribution*, International Conference of Experimental and Numerical Investigations and New Technologies, Zlatibor, Serbia, 29 Jun–2 July 2021.

4. N. Stupar, A. Vranić, A. Stojić, G. Vuković, **D. Vudragović**, D. Maletić, and M. Mitrović Dankulov,, *Spatio-temporal analysis of mobility patterns in the city of Belgrade*, International Conference of Experimental and Numerical Investigations and New Technologies, Zlatibor, Serbia, 29 Jun–2 July 2021.

5. **D. Vudragović**, and A. Balaž *Faraday and Resonant Waves in Dipolar Cigar-Shaped Bose-Einstein Condensates*, Exploring Quantum Many-Body Physics with Ultracold Atoms and Molecules, Online, 14-18 December 2020.

Списак објављених радова и других публикација

Монографска студија/поглавље у књизи М11 или рад у тематском зборнику водећег међународног значаја (М13)

1. S. Stanišić, M. Perišić, G. Jovanović, D. Maletić, **D. Vudragović**, A. Vranić, and A. Stojić, *What Information on Volatile Organic Compounds Can Be Obtained from the Data of a Single Measurement Site Through the Use of Artificial Intelligence?*, Artificial Intelligence: Theory and Applications, Ed. Endre Pap, p. 207-225, Springer (2021),
DOI: 10.1007/978-3-030-72711-6_12.

2. **D. Vudragović**, and A. Balaž, *Science gateway for the Serbian condensed matter physics community*, Science gateways for distributed computing infrastructures, Ed. Peter Kacsuk, p. 209-220, Springer (2014),
DOI: 10.1007/978-3-319-11268-8.

Радови у међународним часописима изузетних вредности (М21а)

1. R. Ravisankar, **D. Vudragović**, P. Muruganandam, A. Balaž, and S. K. Adhikari, *Spin-1 Spin-orbit- and Rabi-coupled Bose-Einstein Condensate Solver*, Comput. Phys. Commun. **259**, 107657 (2021),
DOI: 10.1016/j.cpc.2020.107657; IF(2021) = 4.717.

2. Luis E. Young-S., P. Muruganandam, S. K. Adhikari, V. Lončar, **D. Vudragović**, and A. Balaž, *OpenMP GNU and Intel Fortran programs for solving the time-dependent Gross-Pitaevskii equation*, Comput. Phys. Commun. **220**, 503 (2017),
DOI: 10.1016/j.cpc.2017.07.013; IF(2017) = 3.748.

3. Luis E. Young-S., **D. Vudragović**, P. Muruganandam, S. K. Adhikari, and A. Balaž, *OpenMP Fortran and C programs for solving the time-dependent Gross-Pitaevskii equation in an anisotropic trap*, Comput. Phys. Commun. **204**, 209 (2016),
DOI: 10.1016/j.cpc.2016.03.015; IF(2016) = 3.936.

4. R. K. Kumar, Luis E. Young-S., **D. Vudragović**, A. Balaž, P. Muruganandam, and S. K. Adhikari, *Fortran and C programs for the time-dependent dipolar Gross-Pitaevskii equation in an anisotropic trap*, Comput. Phys. Commun. **195**, 117 (2015),
DOI: 10.1016/j.cpc.2015.03.024; IF(2015) = 3.635.

5. **D. Vudragović**, I. Vidanović, A. Balaž, P. Muruganandam, and S. K. Adhikari, *C Programs for solving the time-dependent Gross-Pitaevskii equation in a fully anisotropic trap*, Comput. Phys. Commun. **183**, 2021 (2012),
DOI: 10.1016/j.cpc.2009.04.015; IF(2012) = 3.078.

Радови у врхунским међународним часописима (М21)

1. B. P. Marinković, V. Vujčić, G. Sushko, **D. Vudragović**, S. Đorđević, S. Ivanović, M. Nešić, D. Jevremović, A. V. Solov'yov, and N. J. Mason, *Development of collisional data base for elementary processes of electron scattering by atoms and molecules*, Nucl. Instrum. Meth. B **354**, 90 (2015),

DOI: 10.1016/j.nimb.2014.12.039, IF(2015) = 1.389.

2. A. Balaž, I. Vidanović, D. Stojiljković, **D. Vudragović**, A. Belić, and A. Bogojević, *SPEEDUP code for calculation of transition amplitudes via the effective action approach*, Commun. Comput. Phys. **11**, 739 (2012), DOI: 10.4208/cicp.131210.180411a, IF(2012) = 1.863.

3. A. Balaž, O. Prnjat, **D. Vudragović**, V. Slavnić, I. Liabotis, E. Atanassov, B. Jakimovski, and M. Savić, *Development of Grid e-Infrastructure in South-Eastern Europe*, J. Grid Comput. **9**, 135 (2011), DOI: 10.1007/s10723-011-9185-0, IF(2011) = 1.310.

Радови у истакнутим међународним часописима (М22)

1. **D. Vudragović**, and A. Balaž, *Faraday and Resonant Waves in Dipolar Cigar-Shaped Bose-Einstein Condensates*, Symmetry **11**, 1090 (2019), DOI: 10.3390/sym11091090; IF(2018) = 2.143.

Радови у међународним часописима (М23)

1. **D. Vudragović**, L. Ilić, P. Jovanović, S. Ničković, A. Bogojević, and A. Balaž, *VI-SEEM DREAMCLIMATE Service*, Scal. Comput. Pract. Exp. **19**, 215 (2018), DOI: 10.12694/scpe.v19i2.1396.

Саопштења са међународних скупова штампана у целини (М33)

1. **D. Vudragović**, P. Jovanović, and A. Balaž, *VI-SEEM virtual research environment*, The 10th RO-LCG Conference, Sinaia, Romania, 26-28 October 2017.

2. J. Lappalainen, **D. Vudragović**, A. Balaž, F. Ruggieri, R. Barbera, R. Lovas, G. Stoitsis, and K. Kastrantas, *Federating computation and storage resources to support agricultural science communities*, EFITA-WCCA-CIGR conference, Turin, Italy, 24-27 June 2013.

Саопштења са међународних скупова штампана у изводу (М34)

1. **D. Vudragović**, *Faraday and Resonant Waves in Dipolar Cigar-Shaped Bose-Einstein Condensates*, The 8th International School and Conference on Photonics, Belgrade, Serbia, 23-27 August 2021.

2. M. Perišić, A. Stojić, G. Jovanović, A. Šoštarić, D. Maletić, **D. Vudragović**, and S. Stanišić, *The potential for forecasting the particulate matter levels in complex urban environment*, International Conference of Experimental and Numerical Investigations and New Technologies, Zlatibor, Serbia, 29 Jun–2 July 2021.

3. S. Stanišić, M. Perišić, A. Stojić, A. Šoštarić, **D. Vudragović**, D. Maletić, and G. Jovanović, *The impact of gaseous pollutants on particulate matter distribution*, International Conference of Experimental and Numerical Investigations and New Technologies, Zlatibor, Serbia, 29 Jun–2 July 2021.

4. N. Stupar, A. Vranić, A. Stojić, G. Vuković, **D. Vudragović**, D. Maletić, and M. Mitrović Dankulov,, *Spatio-temporal analysis of mobility patterns in the city of Belgrade*, International Conference of Experimental and Numerical Investigations

and New Technologies, Zlatibor, Serbia, 29 Jun–2 July 2021.

5. **D. Vudragović**, and A. Balaž *Faraday and Resonant Waves in Dipolar Cigar-Shaped Bose-Einstein Condensates*, Exploring Quantum Many-Body Physics with Ultracold Atoms and Molecules, Online, 14-18 December 2020.

6. **D. Vudragović**, V. Veljić, I. Vasić, and A. Balaž, *Ground state and collective modes of dipolar BECs*, The 7th International School and Conference on Photonics, Belgrade, Serbia, 26-30 August 2019.

7. V. Lončar, **D. Vudragović**, S. K. Adhikari, and A. Balaž, *Parallel solvers for dipolar Gross-Pitaevskii equation*, The 6th International School and Conference on Photonics, Belgrade, Serbia, 28 August - 1 September 2017.

8. V. Lončar, **D. Vudragović**, A. Balaž, and A. Pelster, *Rosensweig instability due to three-body interaction or quantum fluctuations?*, DPG Spring Meeting 2016, Hannover, Germany, 29 February - 4 March 2016.

9. **D. Vudragović**, and A. Balaž, *Faraday waves in dipolar Bose-Einstein condensates*, The 19th Symposium on Condensed Matter Physics - SFKM 2015, Belgrade, Serbia, 7-11 September 2015.

10. **D. Vudragović**, and A. Balaž, *Faraday waves in dipolar Bose-Einstein condensates*, The 5th International School and Conference on Photonics, Belgrade, Serbia, 24-28 August 2015.

11. V. Lončar, **D. Vudragović**, A. Balaž, and A. Pelster, *Faraday waves in dipolar Bose-Einstein condensates*, DPG Spring Meeting 2015, Heidelberg, Germany, 23-27 March 2015.

Spin-1 spin–orbit- and Rabi-coupled Bose–Einstein condensate solver☆,☆☆

Rajamanickam Ravisankar [a], Dušan Vudragović [b], Paulsamy Muruganandam [a,c], Antun Balaž [b], Sadhan K. Adhikari [d,*]

[a] *Department of Physics, Bharathidasan University, Palkalaiperur Campus, Tiruchirappalli 620024, Tamil Nadu, India*
[b] *Institute of Physics Belgrade, University of Belgrade, Pregrevica 118, 11080 Belgrade, Serbia*
[c] *Department of Medical Physics, Bharathidasan University, Palkalaiperur Campus, Tiruchirappalli 620024, Tamil Nadu, India*
[d] *Instituto de Física Teórica, UNESP – Universidade Estadual Paulista, 01.140-70 São Paulo, São Paulo, Brazil*

ARTICLE INFO

ABSTRACT

We present OpenMP versions of FORTRAN programs for solving the Gross–Pitaevskii equation for a harmonically trapped three-component spin-1 spinor Bose–Einstein condensate (BEC) in one (1D) and two (2D) spatial dimensions with or without spin–orbit (SO) and Rabi couplings. Several different forms of SO coupling are included in the programs. We use the split-step Crank–Nicolson discretization for imaginary- and real-time propagation to calculate stationary states and BEC dynamics, respectively. The imaginary-time propagation programs calculate the lowest-energy stationary state. The real-time propagation programs can be used to study the dynamics. The simulation input parameters are provided at the beginning of each program. The programs propagate the condensate wave function and calculate several relevant physical quantities. Outputs of the programs include the wave function, energy, root-mean-square sizes, different density profiles (linear density for the 1D program, linear and surface densities for the 2D program). The imaginary- or real-time propagation can start with an analytic wave function or a pre-calculated numerical wave function. The imaginary-time propagation usually starts with an analytic wave function, while the real-time propagation is often initiated with the previously calculated converged imaginary-time wave function.

Program summary

Program title: BEC-GP-SPINOR, consisting of: BEC-GP-SPINOR-OMP package, containing programs spin-SO-imre1d-omp.f90 and spin-SO-imre2d-omp.f90, with util.f90.

CPC Library link to program files: https://doi.org/10.17632/j3wr4wn946.1

Licensing provisions: Apache License 2.0

Programming language: OpenMP FORTRAN. The FORTRAN programs are tested with the GNU, Intel, PGI, and Oracle compiler.

Nature of problem: The present Open Multi-Processing (OpenMP) FORTRAN programs solve the time-dependent nonlinear partial differential Gross–Pitaevskii (GP) equation for a trapped spinor Bose–Einstein condensate, with or without spin–orbit coupling, in one and two spatial dimensions.

Solution method: We employ the split-step Crank–Nicolson rule to discretize the time-dependent GP equation in space and time. The discretized equation is then solved by imaginary- or real-time propagation, employing adequately small space and time steps, to yield the solution of stationary and non-stationary problems, respectively.

---

1. Introduction

Previously published FORTRAN [1] and C [2] programs are now popular tools for studying the properties of a Bose–Einstein condensate (BEC) by solving the Gross–Pitaevskii (GP) equation and are enjoying widespread use. These programs have later been extended to the more complex scenario of dipolar atoms [3] and of rotating BECs [4]. The OpenMP [5,6] and CUDA [7–9] version of these programs, designed to make these faster and more efficient in multi-core computers, are also available.

There has been great interest in the studies of spinor BECs using the GP equation after the experimental observation of the same [10,11]. Later, it has been possible to introduce an artificial synthetic spin–orbit (SO) coupling by Raman lasers that coherently couple the spin-component states in a pseudo spin-1/2 [12,13] and spin-1 [14] spinor BEC. In this paper, we present new OpenMP FORTRAN programs to solve the GP equation for a three-component spin-1 spinor quasi-one-dimensional (quasi-1D) and quasi-two-dimensional (quasi-2D) BECs [15] with [16,17] or without [18,19] SO and associated Rabi couplings, based on our earlier programs [5,6]. The GP equation for an SO-coupled three-component spin-1 trapped BEC is conveniently solved by the imaginary- and real-time propagation methods. We provide combined imaginary- and real-time programs in one and two spatial dimensions. The present imaginary-time programs already involve complex variables and are hence combined together with the real-time programs, requiring complex algebra. The choice of the type of propagation (imaginary- or real-time) is made through an input parameter. The imaginary-time approach should be used to solve the GP equation for stationary states. A subsequent study of the non-stationary dynamics of the BEC should be done using the real-time propagation using the imaginary-time wave function as the initial state. We use the split-step Crank–Nicolson scheme for solving the GP equation, as in Refs. [1,2].

In Section 2 we present the GP equation for a spin-1 spinor BEC in a trap. The mean-field model and a general scheme for its numerical solution are considered for both quasi-1D and quasi-2D traps. The details about the computer programs, and their input parameters, output files, etc. are given in Section 3. The numerical method and results are given in Section 4, where we illustrate the results for density and energy by employing the imaginary-time propagation for different interaction strengths (nonlinearities). The stability of the density profiles is demonstrated in real-time propagation using the corresponding converged solution obtained by the imaginary time propagation as the initial state. Finally, a brief summary is given in Section 5. Technical and mathematical details of this investigation are presented in two Appendices. A novel numerical procedure applied in this study is given in Appendix A. Useful analytic variational and Thomas–Fermi (TF) approximations are developed in the Supplementary material.

2. The Gross–Pitaevskii equation for a spin-1 condensate

In the mean-field approximation a quasi-1D or quasi-2D SO and Rabi coupled spin-1 ($F = 1$) BEC is described by the following set of three coupled GP equations, for N atoms of mass $\tilde{m}$ each, in dimensionless form, for the spin components $F_z = \pm 1, 0$ [18–20]

$$i\partial_t \psi_{\pm 1}(\mathbf{r}) = \left[-\frac{1}{2}\nabla^2 + V(\mathbf{r}) + c_0\rho + c_2\left(\rho_{\pm 1} - \rho_{\mp 1} + \rho_0\right) \right]\psi_{\pm 1}(\mathbf{r}) + \left\{ c_2\psi_0^2(\mathbf{r})\psi_{\mp 1}^*(\mathbf{r}) \right\} + \frac{\Omega}{\sqrt{2}}\psi_0(\mathbf{r}) + \gamma f_{\pm 1}, \tag{1}$$

$$i\partial_t \psi_0(\mathbf{r}) = \left[-\frac{1}{2}\nabla^2 + V(\mathbf{r}) + c_0\rho + c_2\left(\rho_{+1} + \rho_{-1}\right) \right]\psi_0(\mathbf{r}) + \left\{ 2c_2\psi_{+1}(\mathbf{r})\psi_{-1}(\mathbf{r})\psi_0^*(\mathbf{r}) \right\} + \frac{\Omega}{\sqrt{2}}\sum_{j=+1,-1}\psi_j(\mathbf{r}) + \gamma g, \tag{2}$$

where $\rho_j = |\psi_j|^2$ are the densities of components $j = \pm 1, 0$, and $\rho(\mathbf{r}) = \sum \rho_j(\mathbf{r})$ is the total density, $V(\mathbf{r})$ is the confining trap, ∂_t ($\partial_{\mathbf{r}} \equiv \{\partial_x, \partial_y, \partial_z\}$) is the partial time (space) derivative, and Ω (γ) is the strength of Rabi (SO) coupling. The SO coupling is a space derivative coupling described by the functions f and g, the details of which are given below. For brevity, the time dependence of the wave functions is not explicitly shown in Eqs. (1) and (2). In 1D, $\mathbf{r} = x$, $\nabla^2 = \partial_x^2 = \partial^2/\partial x^2$, in 2D, $\mathbf{r} = \{x, y\}$, $\nabla^2 = \partial_x^2 + \partial_y^2$, and in 3D, $\mathbf{r} = \{x, y, z\}$, $\nabla^2 = \partial_x^2 + \partial_y^2 + \partial_z^2$. In 3D, distances are expressed in units of the harmonic oscillator length $l \equiv \sqrt{\hbar/\tilde{m}\omega}$, density ρ_j in units of l^{-3} and time in units of ω^{-1}, where $\omega = \omega_x$ is the x-axis trapping frequency. The potential is $V(\mathbf{r}) = (x^2 + \kappa^2 y^2 + \beta^2 z^2)/2$, where the trap aspect ratios are $\kappa = \omega_y/\omega$ and $\beta = \omega_z/\omega$. The dimensionless nonlinearities are $c_i = 4\pi N\mathcal{A}_i$, $i = 0, 2$, where $\mathcal{A}_0 = (a_0 + 2a_2)/3l$, $\mathcal{A}_2 = (a_2 - a_0)/3l$, with a_0 and a_2 being the scattering lengths in the total spin channels 0 and 2, respectively. For a pancake-shaped trap, with the strong trapping in z direction ($\beta \gg 1, \kappa$), a set of quasi-2D [15] equations can be obtained with $c_i = 2\sqrt{2\pi\beta}N\mathcal{A}_i$, with $V(\mathbf{r}) = (x^2 + \kappa^2 y^2)/2$. For a cigar-shaped trap, with the strong trapping in y and z directions ($\beta, \kappa \gg 1$), a set of quasi-1D [15] equations can be obtained with $c_i = 2\sqrt{\kappa\beta}N\mathcal{A}_i$, where $V(\mathbf{r}) = x^2/2$. In the following we will take $\kappa = 1$ and $V(\mathbf{r}) = \mathbf{r}^2/2$ in both 1D and 2D. In the programs the parameter κ in the potential is set to unity, but a different value can be introduced easily if needed.

In the presence of the SO coupling [16,17], we consider below the SO-coupling contributions $\gamma f_{\pm 1}$ and γg of Eqs. (1) and (2) in different cases. In 1D we consider three possible SO couplings in the Hamiltonian: $\gamma p_x \Sigma_x$, $\gamma p_x \Sigma_y$, and $\gamma p_x \Sigma_z$, where $p_x = -i\partial_x$ is the momentum operator and Σ_x, Σ_y and Σ_z are the irreducible representations of the x, y and z components of the spin-1 matrix Σ, with components

$$\Sigma_x = \frac{1}{\sqrt{2}}\begin{pmatrix} 0 & 1 & 0 \\ 1 & 0 & 1 \\ 0 & 1 & 0 \end{pmatrix}, \quad \Sigma_y = \frac{i}{\sqrt{2}}\begin{pmatrix} 0 & -1 & 0 \\ 1 & 0 & -1 \\ 0 & 1 & 0 \end{pmatrix}, \quad \Sigma_z = \begin{pmatrix} 1 & 0 & 0 \\ 0 & 0 & 0 \\ 0 & 0 & -1 \end{pmatrix}. \tag{3}$$

For the SO coupling $\gamma p_x \Sigma_x$ [21,22] in 1D, the SO coupling terms in Eqs. (1), (2) are $\gamma f_{\pm 1} = -i\tilde{\gamma}\partial_x\psi_0(\mathbf{r})$ and $\gamma g = -i\tilde{\gamma}\left[\partial_x\psi_{+1}(\mathbf{r}) + \partial_x\psi_{-1}(\mathbf{r})\right]$, respectively, where $\tilde{\gamma} = \gamma/\sqrt{2}$. For the SO coupling $\gamma p_x \Sigma_y$ they are $\gamma f_{\pm 1} = \mp i\tilde{\gamma}\partial_x\psi_0(\mathbf{r})$ and $\gamma g = i\tilde{\gamma}\left[\partial_x\psi_{+1}(\mathbf{r}) - \partial_x\psi_{-1}(\mathbf{r})\right]$, respectively. For the SO coupling $\gamma p_x \Sigma_z$ they are [22] $\gamma f_{\pm 1} = \mp i\gamma\partial_x\psi_{\pm 1}(\mathbf{r})$ and $\gamma g = 0$, respectively.

In 2D we consider the general SO coupling term in the form $\gamma(\eta p_y \Sigma_x - p_x \Sigma_y)$, where $\eta = 1, -1$ and 0 for Rashba [23], Dresselhaus [24] and an equal mixture of Rashba and Dresselhaus SO couplings. In Eqs. (1), (2), the Rashba, Dresselhaus and an equal

mixture of Rashba and Dresselhaus coupling terms in 2D are $\gamma f_{\pm 1} = -i\widetilde{\gamma}\left[\eta\partial_y\psi_0(\mathbf{r})\pm i\partial_x\psi_0(\mathbf{r})\right]$ and $\gamma g = -i\widetilde{\gamma}\left[-i\partial_x\psi_{+1}(\mathbf{r})+i\partial_x\psi_{-1}(\mathbf{r})+\eta\partial_y\psi_{+1}(\mathbf{r})+\eta\partial_y\psi_{-1}(\mathbf{r})\right]$.

The normalization and magnetization (m) conditions are given by

$$\int \rho(\mathbf{r})\,d\mathbf{r} = 1, \quad \text{and} \quad \int \left[\rho_{+1}(\mathbf{r}) - \rho_{-1}(\mathbf{r})\right] d\mathbf{r} = m. \tag{4}$$

Condition (4) is useful to solve the problem for a fixed normalization when magnetization m along z direction is conserved, e.g., when the Hamiltonian commutes with spin-matrix Σ_z. However, in the presence of an SO coupling, that does not commute with Σ_z, magnetization is not conserved due to spin mixing dynamics involving spin-up and down states. In that case, time propagation is performed by imposing only the condition of conservation of normalization without fixing the magnetization during time propagation [25] and it leads to the result for the dynamically stable stationary state with a magnetization determined by the parameters of the model, which could often be zero. In this context, it should be noted that in experiments it is not possible to fix a preassigned value to magnetization, which is not a constant of motion.

The energy functional of the system is [18,19]

$$\begin{aligned}
E = \frac{1}{2}\int d\mathbf{r} &\left\{ \sum_j |\nabla_{\mathbf{r}}\psi_j|^2 + 2V(\mathbf{r})\rho + c_0\rho^2 \right. \\
&+ c_2\left[\rho_{+1}^2 + \rho_{-1}^2 + 2\left(\rho_{+1}\rho_0 + \rho_{-1}\rho_0 - \rho_{+1}\rho_{-1} + \psi_{-1}^*\psi_0^2\psi_{+1}^* + \psi_{-1}\psi_0^{*2}\psi_{+1}\right)\right] \\
&+ 2\frac{\Omega}{\sqrt{2}}\left[(\psi_{+1}^* + \psi_{-1}^*)\psi_0 + \psi_0^*(\psi_{+1} + \psi_{-1})\right] + 2\gamma\left[\psi_{+1}^*f_{+1} + \psi_{-1}^*f_{-1} + \psi_0^*g\right]\right\}.
\end{aligned} \tag{5}$$

3. Details about the programs

We use the split time step Crank–Nicolson discretization rule for solving the GP equations (1) and (2), including the appropriate SO and Rabi couplings with strengths γ and Ω, respectively. This approach has been elaborated in detail in Ref. [1]. An initial (known) wave function at time t is used to calculate the wave function at time $t + \Delta$, after a small time step Δ. The advantage of this approach lies in the fact that different terms on the right-hand-side of Eqs. (1) and (2) can be treated successively. For example, the spatial derivative term involving $\nabla_{\mathbf{r}}$ can be treated independently of the nonlinear interaction terms and also of the SO and Rabi coupling terms. The terms in the square brackets of Eqs. (1) and (2) can be treated in a routined way elaborated in Ref. [1]. The terms in the curly brackets and those proportional to Ω in Eqs. (1) and (2) need special attention and are treated as in Appendix A. Finally, the γ-dependent SO coupling terms only involve first order space derivatives and are treated in a routined fashion.

The presented programs are straightforward modifications of the basic programs published in Refs. [1,2]. The three components of the wave function are accommodated by introducing a new index "L" in addition to the space indices in the corresponding arrays, i.e., the wave-function components are represented by CP(L,I,J) in 2D and CP(L,I) in 1D, where L = 1, 2, 3 stands for the spin components $j = +1$, 0, and -1, respectively, and I and J denote discretized space points. The time propagation with respect to different terms in Eqs. (1) and (2) are dealt with in different subroutines. The kinetic energy term ($\nabla^2/2$) is treated using the Crank–Nicolson discretization in subroutines COEF, LUX, and LUY in 2D, and in 1D in subroutines COEF and LU, as in Refs. [1,2]. The potential term and the diagonal part of the nonlinear terms in square brackets, proportional to c_0 and c_2, are treated in the subroutine CALCNU. The off-diagonal part of the nonlinear terms in curly brackets in Eqs. (1) and (2), explicitly considered in Eq. (A.1), is treated in the subroutine HERM, while the different SO coupling terms are treated in the subroutine SO. The conservation of the normalization and magnetization, as defined by Eqs. (A.6) and (A.7), is implemented in the subroutine RENORM. The energies are calculated in the subroutine ENERGY and expectation values of the condensate's cloud sizes are calculated in the subroutine RADIUS in 2D and LENGTH in 1D. The different modules (Subroutines and Functions) of the programs in 1D and 2D and their respective usage are presented in Table 1.

A description of the input parameters together with the output files with description is given in Table 2. Most of the parameters have the same meaning as in our previously published programs and the reader can refer to Ref. [6] for details. For an efficient performance on computers with multiple CPU cores, the programs have been parallelized using the OpenMP library. The number of threads (CPU cores) to be used is declared by the parameter NTHREADS, which should be equal to or less than the total number of available threads. If NTHREADS is set to zero, then all available CPU cores will be used. The parameters NSTP, NPAS, and NRUN denote different numbers of time iterations, the total number of iterations being the sum of these. If NSTP is different from zero, then the program starts the time propagation using an analytic initial function defined in the subroutine INITIALIZE. If NSTP is zero, the program reads an initial wave function for the calculation from input files, i.e., from the previously calculated files named `<code>-wave-fun-fin.txt`. In this way one can perform the imaginary- or real-time propagation with a pre-calculated wave function. The supplied programs use the pre-defined value `NSTP = 10` and use an analytic wave function as the initial state. When using a pre-calculated wave function by setting NSTP to zero, the number of space grid points N (1D) and NX, NY (2D) employed previously should match exactly the number of points used in the current program. The supplied programs assume equal numbers of space step points in both imaginary- and real-time propagation. The parameter OPT_SO selects the type of SO coupling. In 1D, OPT_SO = 1, 2, 3 uses the SO couplings $\gamma p_x \Sigma_x$, $\gamma p_x \Sigma_y$, and $\gamma p_x \Sigma_z$, respectively. In 2D, OPT_SO = 1, 2, 3 uses Rashba, Dresselhaus, and an equal mixture of Rashba and Dresselhaus SO couplings, respectively. The choice OPT_SO = 0 corresponds to no SO coupling. The parameters MAG_0, GAM0 (GAMMA0 in 1D) and OMEGA0 denote magnetization, the strength of SO coupling γ and that of Rabi coupling Ω, respectively. The parameter OPT_PROP selects the type of time propagation: imaginary-time (1) and real-time (2). All input data are conveniently placed at the beginning of each program, as before [5]. After changing the input data in a program a recompilation is required. The output files are conveniently named such that their contents can be easily identified, following the naming convention introduced in Ref. [5]. For example, a file named `<code>-out.txt`, where `<code>` denotes imaginary- (im) or real-time (re) propagation, represents the general output file

Table 1
Different modules of the 1D and 2D programs and their usage.

	Module name	Type	Usage
1D	IMRE1D	MAIN	Main program
	INITIALIZE	Subroutine	Calculates or reads the initial function
	CALC_TRAP	Subroutine	Calculates the confining trap
	COEF	Subroutine	Calculates the coefficients of the Crank–Nicolson method
	SO	Subroutine	Propagates the spin–orbit coupling term in time
	LU	Subroutine	Crank–Nicolson time propagation
	HERM	Subroutine	Propagates the off-diagonal terms of the GP equation and the Rabi coupling term in time
	CALCNU	Subroutine	Propagates the diagonal parts of the GP equation in time
	LENGTH	Subroutine	Calculates the length of the condensate
	RENORM	Subroutine	Fixes the normalization and magnetization
	ENERGY	Subroutine	Calculates the energy of the condensate
	SIMP	Function	Performs integration by Simpson's rule
2D	IMRE2D	MAIN	Main program
	INITIALIZE	Subroutine	Calculates or reads the initial function
	CALC_TRAP	Subroutine	Calculates the confining trap
	COEF	Subroutine	Calculates the coefficients of the Crank–Nicolson method
	SO	Subroutine	Propagates the spin–orbit coupling term in time
	LUX	Subroutine	Crank–Nicolson time propagation in x variable
	LUY	Subroutine	Crank–Nicolson time propagation in y variable
	HERM	Subroutine	Propagates the off-diagonal terms of the GP equation and the Rabi coupling term in time
	CALCNU	Subroutine	Propagates the diagonal parts of the GP equation in time
	INTEGRATE	Function	Performs double integration in x and y
	RADIUS	Subroutine	Calculates the radius of the condensate
	RENORM	Subroutine	Fixes the normalization and magnetization
	ENERGY	Subroutine	Calculates the energy of the condensate
	SIMP	Function	Performs integration by Simpson's rule

Table 2
Name and description of input parameters and output files.

	Name	Description
Input	NSTP, NPAS, NRUN	Number of time iterations, NSTP = 0 reads initial function, NSTP > 0 calculates initial function
	N, NX, NY	Number of space integration points
	NTHREADS	Number of threads used NTHREADS = 0 uses all threads
	C_0, C_2	Nonlinear input parameters (c_0, c_2)
	OPT_SO	Selects the type of SO coupling
	DX, DY	Space discretization steps
	OPT_PROP	Selects the type of time propagation imaginary-time (=1) or real-time (=2)
	OPT_ST	Selects initial function in 2D
	MAG_0	Magnetization (m)
	GAM0	Strength of SO coupling (γ)
	OMEGA0	Strength of Rabi coupling (Ω)
Output	im-out.txt	Input parameters, energy and size
	im-den-<desc>.txt	<desc>=ini initial & =fin final density
	im-phase.txt	phase of a 2D wave function
	im-wave-fun-<desc>.txt	<desc>=ini initial & =fin final wave function
	im-den-rad-<desc>.txt	<desc>=ini initial & =fin final radial density (2D)

containing input data, space and time steps DX, DY and DT, nonlinearity c_0 and c_2, energy, size, etc. The files `<code>-den-ini.txt` and `<code>-den-fin.txt` contain the initial and final components and total densities in different columns. In 1D (2D) these densities are functions of one (two) space point(s) placed in the first (and second) column(s) of the respective files. The densities ρ_{+1}, ρ_0, ρ_{-1}, and ρ can be found in the successive columns. The file `<code>-den-rad-fin.txt` stores the final linear radial densities ρ_{+1}, ρ_0, ρ_{-1}, and ρ for the 2D GP equation in different columns, while the space points are saved in the first column. The file `<code>-wave-fun-fin/ini.txt` contains the final/initial complex wave functions. For a 2D BEC, the file `<code>-phase.txt` contains the phases of the component wave functions in different columns, since the phase is important for the study of angular momentum of the respective states. The printing of some of these files, such as the initial density and wave function, is commented out in the programs, so that the supplied programs do not print these.

We provide below the beginning of the 1D program where the parameters are defined so that the reader can easily identify the different statements there. The 2D program is quite similar.

```
! Begin selection of input parameters
MODULE COMM_DATA
! SELECT # OF SPACE POINTS N AND # OF TIME ITERATIONS NSTP, NPAS & NRUN
! USE NSTP = 0 TO READ WAVE FUNCTION FILE FROM STDIN: < im-wave-fun-fin.txt
```

```
  INTEGER, PARAMETER :: N = 640, NX = N-1, NX2 = N/2
  INTEGER, PARAMETER :: NSTP = 10, NPAS = 1000000, NRUN = 100000
! INTEGER, PARAMETER :: NSTP = 0, NPAS = 1000000, NRUN = 100000
! Number of OpenMP threads, less than or equal to the maximum available cores.
  INTEGER, PARAMETER  :: NTHREADS = 0  ! NTHREADS = 0 uses all available cores
  REAL (8), PARAMETER :: Pi = 3.14159265358979D0
END MODULE COMM_DATA
!************************************************************
MODULE SPIN_PARS
 USE COMM_DATA, ONLY : PI
!****** SELECT  POLAR (C_2 > 0) OR FERROMAGNETIC (C_2 < 0) BEC ******
! REAL (8), PARAMETER :: C_0 = 241.d0, C_2 = 7.5d0 ! Anti-ferromagnetic
  REAL (8), PARAMETER :: C_0 = 885.d0, C_2 = -4.1d0  ! Ferromagnetic
END MODULE SPIN_PARS
!************************************************************
MODULE GPE_DATA
 USE COMM_DATA, ONLY : N, Pi
 USE SPIN_PARS, ONLY : C_0, C_2
!********************************************************************
!*** SELECT OPTION FOR SO COUPLING AND STRENGTH GAMMA
! INTEGER,PARAMETER :: OPT_SO = 0; REAL (8), PARAMETER :: GAMMA0 = .00D0 ! No SO coupl.
  INTEGER,PARAMETER :: OPT_SO = 1; REAL (8), PARAMETER :: GAMMA0 = .500D0 ! Sigma_x p_x
! INTEGER,PARAMETER :: OPT_SO = 2; REAL (8), PARAMETER :: GAMMA0 = .500D0 ! Sigma_y p_x
! INTEGER,PARAMETER :: OPT_SO = 3; REAL (8), PARAMETER :: GAMMA0 = .500D0 ! Sigma_z p_x
!********************************************************************
 REAL (8), PARAMETER :: DX = 0.05D0 ! SELECT SPACE STEP DX
!!SELECT OPTION  FOR PROPAGATION: IMAGINARY-TIME or REAL-TIME
 INTEGER, PARAMETER :: OPT_PROP = 1; REAL (8), PARAMETER :: DT = DX*DX*0.10D0 ! IMAG
! INTEGER, PARAMETER :: OPT_PROP = 2; REAL (8), PARAMETER :: DT = DX*DX*0.05D0 ! REAL
!!SELECT PARAMETERS OF MODEL
 REAL (8), PARAMETER :: MAG_0 = .400000D0, ACCUR=1.D-6 ! Magnetization
 REAL (8), PARAMETER :: OMEGA0 = .000D0             ! Rabi and SO coupling
!********************************************************************
! End selection of input parameters
```

Below we provide a sample output file re-out.txt for the 2D program for the readers to familiarize.

```
  REAL-TIME PROPAGATION
  # of threads  =       16

  RASHBA SO coupling, GAMMA =  0.500000000000000
  RABI coupling Omega =  0.000000000000000E+000
  Nonlinearity C_0 = 482.000000, C_2 = 15.000000
  OPT_ST =  0.750000000000000

  Space and time steps: DX = 0.10000,  DY = 0.10000, DT = 0.2500E-03
  # of space steps: NX =  161, NY = 161
  # of time steps:  NSTP = 0, NPAS = 80000, NRUN = 10000


            ---------------------------------------------
             RAD(1)   RAD(2)   RAD(3)   Energy    MAG
            ---------------------------------------------
NSTP iter.:  3.469    2.194    3.469    8.1969    0.0000
NPAS iter.:  3.468    2.193    3.468    8.1969   -0.0000
NRUN iter.:  3.469    2.195    3.469    8.1969   -0.0000
            ---------------------------------------------


 Clock Time:     129 seconds
   CPU Time:    2048 seconds
```

Another crucial aspect for the execution of imaginary-time propagation to find the lowest-energy ground state is a proper choice of initial state with right symmetry property as the final state. Different types of states can be obtained for different sets of parameters. Without SO coupling, the solution is of the Gaussian type and a Gaussian function should be chosen as the initial state. For small Rashba or Dresselhaus SO-coupling strength γ ($\gamma \lesssim 0.75$), the lowest-energy circularly-symmetric state of the three components of a quasi-2D SO-coupled anti-ferromagnetic (polar) spin-1 BEC is of the $(-1, 0, +1)$ or $(+1, 0, -1)$ type, where the numbers in the parenthesis represent the angular momentum of the vortices in the center of the components $j = +1, 0, -1$, respectively, with the
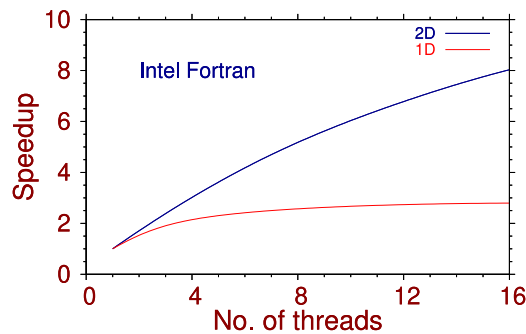
Fig. 1. Speedup of execution on a 20-core machine with two Intel Xeon E5-2650 processors (2×10 CPU cores) versus the number of threads used, for a quasi-1D and quasi-2D BEC for a typical run. The size of the space grid in 1D is 1000 and in 2D it is 200×200. The programs were compiled using the Intel Fortran compiler v. 19.0.4.243.

negative sign representing an anti-vortex. For a ferromagnetic spin-1 quasi-2D BEC these states are of the type $(0, \pm 1, \pm 2)$ for Rashba and Dresselhaus SO-couplings, respectively, in agreement with the consideration of Ref. [26]. For an equal mixture of Rashba and Dresselhaus SO couplings, for small γ, the lowest-energy ferromagnetic BEC states are of the Gaussian type without any vortices; the anti-ferromagnetic BEC states are of the stripe type with periodic 1D modulation in density. For an efficient computation, the vortices or anti-vortices are introduced in the initial wave functions when required. The vortex of angular momentum L is imprinted by taking the initial state as a Gaussian multiplied by the factor $(x + iy)^L$, and an anti-vortex by the factor $(x - iy)^L$. For large SO-coupling strength γ ($\gamma \gtrsim 0.75$), the density of the lowest-energy ground state of the three components of an SO-coupled spinor BEC exhibits different patterns (not considered in this paper). The initial states in the 2D program have to be chosen accordingly. A stripe pattern is generated by multiplying an initial Gaussian state by $\sin(\gamma x)$ and $\cos(\gamma x)$. The user can change the initial state for a SO-coupled BEC by choosing the value of the parameter OPT_ST. For $\gamma <$ OPT_ST the states of type $(\mp 1, 0, \pm 1)$ and $(0, \pm 1, \pm 2)$ are chosen in anti-ferromagnetic and ferromagnetic phases, the upper (lower) sign corresponds to Rashba (Dresselhaus) SO coupling. In the anti-ferromagnetic phase, for $\gamma >$ OPT_ST, the stripe states are chosen as the initial state. However, to reproduce the results reported in this paper there is no need to change the parameter OPT_ST. For an equal mixture of Rashba and Dresselhaus SO couplings Gaussian-type initial states are appropriate for the ferromagnetic phase and stripe states for the anti-ferromagnetic phase.

If the imaginary-time propagation is performed, the programs run either by using an initial analytic input function (if NSTP is not set to zero), or by employing a pre-calculated wave function (if NSTP is set to zero). The real-time propagation can successfully work only if initialized with a meaningful wave function, usually assuming that NSTP = 0 is set, and that the program will read a pre-calculated wave function by the earlier performed imaginary-time propagation. The calculation is essentially done within the NPAS time iteration loop. Another NSTP time iteration is accommodated to verify if the results converged by comparing the energies and sizes after NPAS and NSTP iterations. The source programs spin-SO-imre1d-omp.f90 (1D) and spin-SO-imre2d-omp.f90 (2D) are located in the directory src within the corresponding package directory BEC-GP-SPINOR-OMP. A README.md file, included in the corresponding root directory, explains the procedure to compile and run the programs in more detail using a makefile. In the beginning of each program the compilation commands are given for GNU, Intel, PGI, and Oracle (former Sun) Fortran compilers. They can be compiled by the make command using the provided makefile in the corresponding package root directory. Otherwise, they can be compiled by the commands given at the beginning of the programs using Intel, GNU, PGI, and Oracle FORTRAN compilers. The examples of produced output files can be found in the directory output, although some large density files are omitted, to reduce the software package size.

We conclude this section demonstrating the efficiency of our OpenMP parallelization scheme using the Intel compiler on a machine with 2×10 CPU cores in Fig. 1, where we plot the speedup versus number of threads. The speedup for n threads is defined as the ratio of clock time for a single thread to that for n threads. From Fig. 1 we find the clock time reduces with the increase of the number of threads, thus making the execution more efficient in a multi-core machine.

4. Numerical results

All calculations reported below were performed with the predefined space and time steps DX and DT in the programs: in 1D DX = 0.05, DT = DX*DX*0.1 (imaginary time) and DT = DX*DX*0.05 (real time); in 2D DX = 0.1, DT = DX*DX*0.1 (imaginary time) and DT = DX*DX*0.025 (real time). To increase the accuracy of calculation, the space step(s) DX and DY should be reduced and the total number of space discretization points N, NX, and NY increased proportionally.

The parameters of the GP equation c_0 and c_2 are taken from the following realistic experimental situations. For the ferromagnetic BEC the quasi-1D trap parameters are $l = 2.41927$ μm, $l_{yz} = 0.54$ μm and we use the following parameters of ^{87}Rb atoms: $N = 10,000$, $a_0 = 101.8a_B$, $a_2 = 100.4a_B$, where a_B is the Bohr radius. Consequently, $c_0 \equiv 2N(a_0 + 2a_2)l/3l_{yz}^2 \approx 885$ and $c_2 \equiv 2N(a_2 - a_0)l/3l_{yz}^2 \approx -4.1$. For the quasi-1D anti-ferromagnetic BEC we use the trap parameters $l = 4.7$ μm, $l_{yz} = 1.05$ μm following parameters of ^{23}Na atoms: $N = 10,000$, $a_0 = 50.00a_B$, $a_2 = 55.01a_B$. Consequently, $c_0 \approx 241$ and $c_2 \approx 7.5$. For the quasi-2D ferromagnetic BEC we use the following parameters of ^{87}Rb atoms: $N = 100,000$, $a_0 = 101.8a_B$, $a_2 = 100.4a_B$, [27]$l_z = 2.0157$ μm. Consequently, $c_0 \equiv 2N\sqrt{2\pi}(a_0 + 2a_2)/3l_z \approx 1327.5$ and $c_2 \equiv 2N\sqrt{2\pi}(a_2 - a_0)/3l_z \approx -6.15$. For the quasi-2D anti-ferromagnetic BEC we use the following parameters of ^{23}Na atoms: $N = 100,000$, $a_0 = 50.00a_B$, $a_2 = 55.01a_B$, [28] $l_z = 2.9369$ μm. Consequently, $c_0 \approx 482$ and $c_2 \approx 15$.

Although we will calculate the lowest-energy ground state by imaginary-time propagation, it is possible that in some cases for larger values of SO coupling strength γ (not considered in this paper) the imaginary-time approach may converge to a nearby excited state instead of the lowest-energy ground state for certain initial states. The symmetry, such as parity, of the initial state plays a vital role.

Table 3

Convergence of energies of harmonically trapped 1D and 2D spin-1 ferromagnetic (ferro) and anti-ferromagnetic (polar) BECs with change of space steps DX and DY. The parameters in 1D: $c_0 = 885$, $c_2 = -4.1$ (ferro) and $c_0 = 241$, $c_2 = 7.5$ (polar). The parameters in 2D: $c_0 = 1327.5$, $c_2 = -6.15$ (ferro), $c_0 = 482$, $c_2 = 15$ (polar). The SO-coupled results in 1D refer to the coupling $\gamma p_x \Sigma_x$ with $\gamma = 0.5$ and those in 2D correspond to the Rashba coupling with $\gamma = 0.5$. The parameters considered here are appropriate for a Rb and Na BEC with trap parameters of Ref. [25].

DX (=DY)	1D (ferro) energy	1D (ferro) % error	1D (polar) energy	1D (polar) % error	2D (ferro) energy	2D (ferro) % error	2D (polar) energy	2D (polar) % error
0.4	36.01167	0.00058	15.12364	0.00066	13.59737	0.00176	8.19636	0.00660
0.2	36.01146	0	15.12354	0	13.59759	0.00015	8.19687	0.00037
0.1	36.01146	0	15.12354	0	13.59761	0	8.19690	0
< 0.05	36.01146	0	15.12354	0	13.59761	0	8.19690	0

Table 4

Energies of harmonically-trapped spin-1 anti-ferromagnetic (polar) and ferromagnetic (ferro) quasi-1D and quasi-2D BECs for different values of magnetization m. In the quasi-2D case we consider only the circularly-symmetric states. The parameters in 1D: $c_0 = 241$, $c_2 = 7.5$ (polar) and $c_0 = 885$, $c_2 = -4.1$ (ferro), space step DX = 0.05, time step DT = 0.00025. The parameters in 2D: $c_0 = 482$, $c_2 = 15$ (polar) and $c_0 = 1327.5$, $c_2 = -6.15$ (ferro), space steps DX = DY = 0.1, time step DT = 0.0005. The SO-coupled (SO-cpld) results in 1D refer to the coupling $\gamma p_x \Sigma_x$ with $\gamma = 0.5$ and those in 2D correspond to the Rashba or Dresselhaus coupling with $\gamma = 0.5$. For systems with large nonlinearities the numerically obtained energy E_{num} lies between the TF [29] and variational (var) limit: $E_{TF} < E_{num} < E_{var}$. The parameters considered here are appropriate for a Rb and Na BEC with trap parameters of Ref. [25].

	m	1D spinor	1D spinor [25]	1D spinor var	1D spinor TF	1D SO-cpld $\gamma = 0.5$	2D spinor	2D spinor var	2D spinor TF	2D SO-cpld $\gamma = 0.5$
	0	15.2485	15.2485	15.7522	15.2239	15.1235	8.3605	8.8155	8.2577	8.1969
	0.1	15.2514	15.2514				8.3617			
	0.2	15.2599	15.2599				8.3652			
Polar	0.3	15.2743	15.2743				8.3710			
	0.4	15.2945	15.2945				8.3793			
	0.5	15.3209	15.3209				8.3900			
	0.6	15.3537	15.3537				8.4033			
	0	36.1365	36.1365	37.3574	36.1243	36.0115	13.7420	14.5364	13.6723	
	0.0468	36.1365					13.7420			13.5976
	0.1	36.1365	36.1365				13.7420			
Ferro	0.2	36.1365	36.1365				13.7420			
	0.3	36.1365	36.1365				13.7420			
	0.4	36.1365	36.1365				13.7420			
	0.5	36.1365	36.1365				13.7420			
	0.6	36.1365	36.1365				13.7420			

An even-parity (odd-parity) initial state will find the lowest-energy state with even (odd) parity. For small γ there are only a few possibilities of symmetry and this problem does not appear for the results reported in this paper. But for larger γ, and especially in the quasi-2D case, there are states with many possibilities of symmetry and it may not be easy to know, a priori, the symmetry of the lowest-energy state. Hence, for large γ, it is advised to repeat the calculation with different initial states, so as to be sure that the converged state is indeed the lowest-energy ground state. In fact, any numerically computed final wave function, obtained with the same number of space points, can be used as the initial state for a new calculation.

Before we illustrate our results, we now study in Table 3 the convergence of our calculational scheme in 1D and 2D for SO-coupled ferromagnetic and polar BECs employing the above-mentioned parameters in 1D and 2D upon the reduction of space steps DX and (= DY) from 0.4 to 0.05. In this Table we display the energies, viz. Eq. (5), and the respective percentage numerical errors for four different sets of parameters in 1D and 2D. We see that upon a reduction of space step the energy value rapidly converges. The result for energy with space step 0.4 is already very accurate and the result remains unchanged to five significant figures after the decimal point for
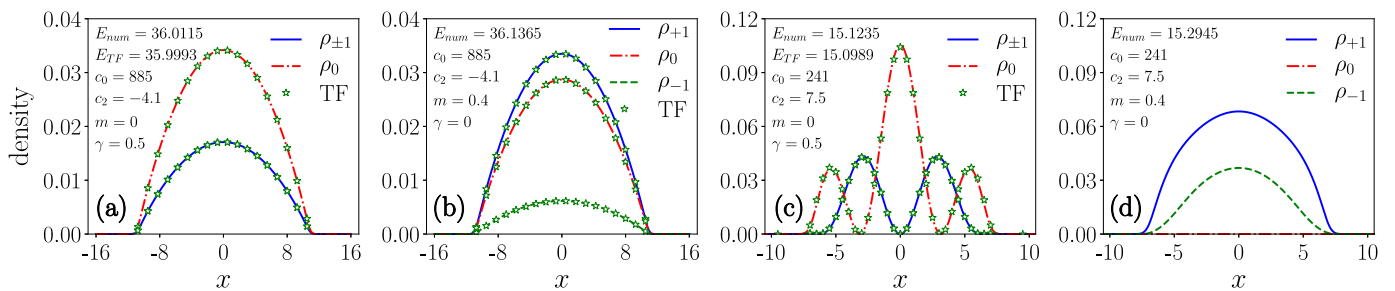

Fig. 2. Numerically calculated component density $\rho_j(x)$ (lines) and energy E of a quasi-1D harmonically trapped SO-coupled ferromagnetic BEC with nonlinearities $c_0 = 885$, $c_2 = -4.1$ and (a) $\gamma = 0.5$ and (b) $m = 0.4$, $\gamma = 0$, compared with the analytic TF result (chain of symbols). The same for an anti-ferromagnetic BEC with nonlinearities $c_0 = 241$, $c_2 = 7.5$ and (c) $\gamma = 0.5$ and (d) $m = 0.4$, $\gamma = 0$. The SO-coupling is $\gamma p_x \Sigma_x$ with $\gamma = 0.5$ in all cases. All densities are calculated by imaginary-time propagation employing Gaussian input functions. All results reported in this paper are in dimensionless units, as outlined in Section 2.
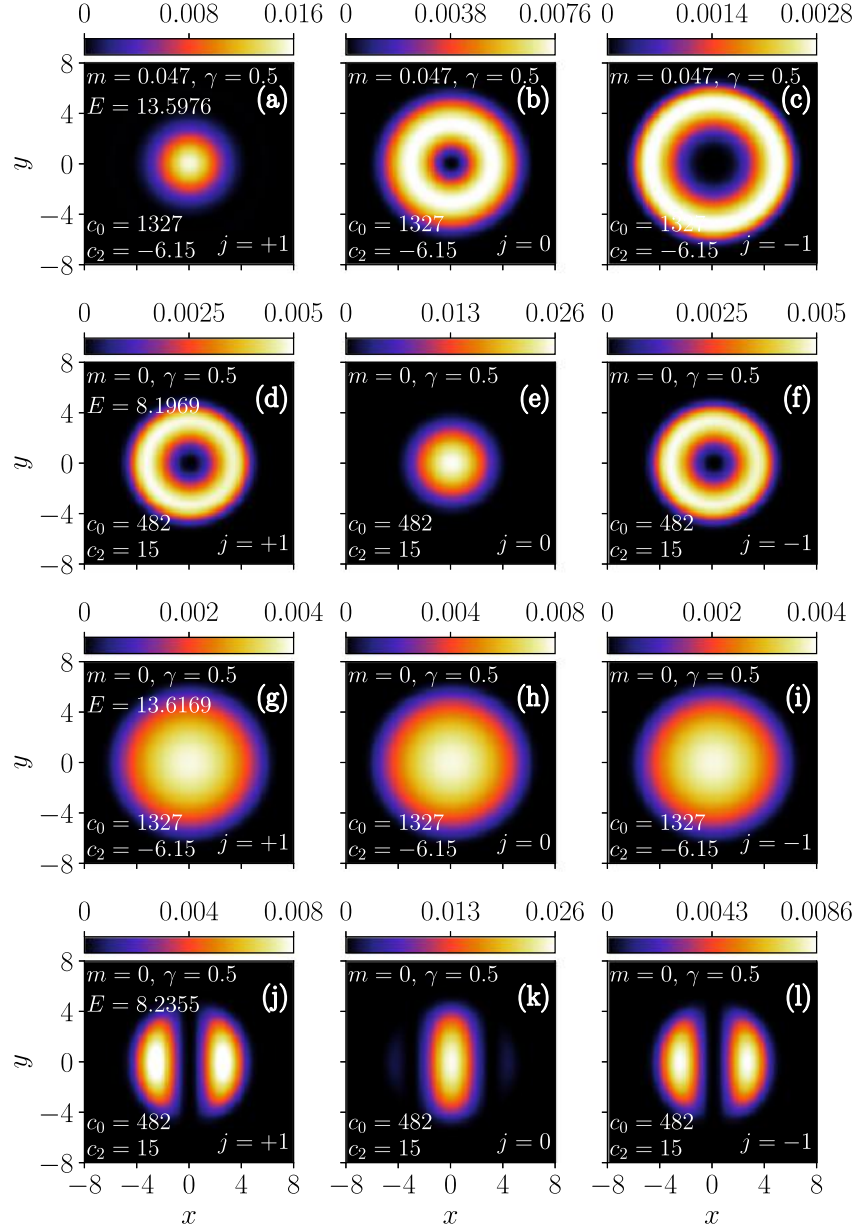
Fig. 3. Contour plots of numerically calculated component densities $\rho_j(x, y)$ for (a) $j = +1$, (b) $j = 0$, and (c) $j = -1$ of a quasi-2D harmonically trapped Rashba or Dresselhaus SO-coupled ferromagnetic BEC with nonlinearities $c_0 = 1327.5$, $c_2 = -6.15$, the SO-coupling strength $\gamma = 0.5$. (d)-(f) A Rashba or Dresselhaus SO-coupled anti-ferromagnetic BEC with nonlinearities $c_0 = 482$, $c_2 = 15$, and $\gamma = 0.5$. (g)-(i) A ferromagnetic BEC with $c_0 = 1327.5$, $c_2 = -6.15$, $\gamma = 0.5$ for an equal mixture of Rashba and Dresselhaus SO couplings. (j)-(l) An anti-ferromagnetic BEC with $c_0 = 482$, $c_2 = 15$, $\gamma = 0.5$ for an equal mixture of Rashba and Dresselhaus SO couplings. The numerical energies are displayed in plots (a), (d), (g), and (j).

space steps 0.1 and 0.05 both in 1D and 2D. In the following we will present results of our study with space steps 0.05 and 0.1 in 1D and 2D, respectively. The accuracy increases as the space-step is reduced, but a reduced value of space step requires a larger number of time iterations for convergence. Hence, it is computationally more economic to use a large space step.

In Table 4 we show the energy, viz. Eq. (1), of an anti-ferromagnetic and a ferromagnetic BEC in quasi-1D and quasi-2D traps for different values of magnetization m. For the quasi-2D trap, we consider only the circularly-symmetric states. In 2D the energies are the same for both Rashba and Dresselhaus SO couplings, although the underlying wave functions are different. The analytic TF and variational energies are also displayed, for comparison, as well as those from Ref. [25]. In the case of a ferromagnetic BEC without SO coupling, the energies are independent of m values, whereas in the anti-ferromagnetic case the dependence on m exists, as can be seen. In both cases the analytic TF and variational energies are independent of m. For condensates with large densities as in Table 4, where the TF results are reliable, the actual energies are larger than the corresponding TF values [29]. On the other hand, the variational energies are always larger than the actual energies. Hence for large nonlinearities, as we see in Table 4, the variational and TF energies define the two bounds for the actual, numerically calculated energy. In Table 4 we also present the numerically calculated energies for the SO-coupled BECs in 1D and 2D for $\gamma = 0.5$.

We show the numerically calculated and the TF component densities $\rho_j(\mathbf{x})$ of a quasi-1D harmonically trapped ferromagnetic SO-coupled BEC for $c_0 = 885$ and $c_2 = -4.1$, with $\gamma = 0.5$ in Fig. 2(a) and $m = 0.4$, $\gamma = 0$ in Fig. 2(b), along with the corresponding
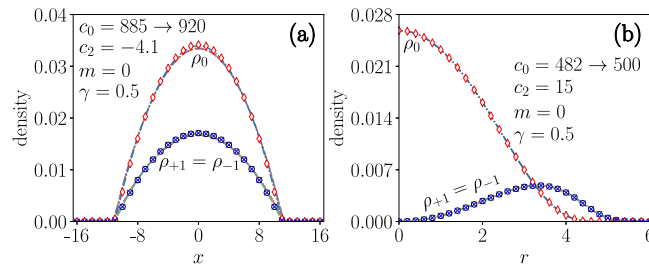
Fig. 4. (a) Numerically calculated component densities of the quasi-1D SO-coupled ferromagnetic BEC of Fig. 2(a) with $c_0 = 885$, $c_2 = -4.1$, $\gamma = 0.5$ during the real-time evolution at times $t = 50, 100, 150, 200$ (full lines), using the imaginary-time wave function as the initial state, compared with the converged imaginary-time densities shown in Fig. 2(a) (chain of symbols). The parameter c_0 was changed from 885 to 920 at $t = 0$. (b) Numerically calculated radial component densities of the quasi-2D anti-ferromagnetic Dresselhaus SO-coupled BEC of Fig. 3(d)–(f) with $c_0 = 482$, $c_2 = 15$, $\gamma = 0.5$ during the real-time evolution at times $t = 50, 100, 150, 200$ (full lines), using the imaginary-time wave function as the initial state, compared with the converged imaginary time densities (chain of symbols). The parameter c_0 was changed from 482 to 500 at $t = 0$.

energy values given by Eq. (5). All the states reported here are the lowest-energy ground states for a given set of parameters, obtained by imaginary-time propagation. The same quantities are shown for an anti-ferromagnetic BEC with $c_0 = 241$ and $c_2 = 7.5$, with $\gamma = 0.5$ in Fig. 2(c) and with $m = 0.4$, $\gamma = 0$ in Fig. 2(d). The SO coupling in both cases is of type $\gamma p_x \Sigma_x$ with $\gamma = 0.5$. These nonlinear parameters c_0 and c_2 were considered previously in Ref. [25]. These states are calculated with the analytic initial functions, included by setting NSTP $\neq 0$.

We now exhibit the density of a Rashba SO-coupled quasi-2D spinor BEC for $\gamma = 0.5$. The BEC components develop distinct angular momentum structure in this case. To illustrate this, we display in Fig. 3(a)–(c) the contour plots of densities of a ferromagnetic Rashba or Dresselhaus SO-coupled BEC. In Fig. 3(d)–(f) the corresponding contour plots of an anti-ferromagnetic Rashba or Dresselhaus SO-coupled BEC are shown, while Fig. 3(g)–(i) displays the same for a ferromagnetic BEC for an equal mixture of Rashba and Dresselhaus couplings. In Fig. 3(j)–(l) the plots are shown for an anti-ferromagnetic BEC, also for an equal mixture of Rashba and Dresselhaus couplings. In all cases the nonlinearities c_0 and c_2 are the same as in Table 3. The components $j = +1, 0$ and -1 in Fig. 3(a)–(c) have angular momentum $0, \pm 1, \pm 2$, respectively, for Rashba and Dresselhaus SO couplings. On the other hand, the components in Fig. 3(d)–(f) have angular momentum $\mp 1, 0, \pm 1$, respectively, for Rashba and Dresselhaus SO couplings. The angular momenta of the spinor components were found from the contour plot of the phases of the corresponding wave functions (not explicitly considered in this paper).

Finally, we demonstrate the dynamical stability of the imaginary-time results using the real-time propagation for a large interval of time. Using the converged imaginary-time wave function as the initial state, the real-time calculation is initiated after introducing a small perturbation, by changing the value of c_0 at $t = 0$ by a small amount. First we consider the quasi-1D SO-coupled ferromagnetic spinor BEC of Fig. 2(a) and perform a real-time simulation for 200 units of time by changing c_0 from 885 to 920. The component densities at times $t = 50, 100, 150$, and 200 are plotted in Fig. 4(a). The imaginary-time converged results (chain of symbols) are also shown, for comparison. Next we consider a quasi-2D anti-ferromagnetic Rashba SO-coupled spinor BEC with $c_0 = 482$, $c_2 = 15$, $\gamma = 0.5$, viz. Fig. 3(d)–(f), which is taken as initial state and a real-time propagation is performed for 200 units of time upon changing c_0 from 482 to 500 at $t = 0$. The radial component densities are plotted at times $t = 50, 100, 150$, and 200 in Fig. 4(b) together with the converged imaginary-time density (chain of symbols). The fact that all component densities in Fig. 4(a) and (b) for a quasi-1D and a quasi-2D BEC over a large interval of time are stable during the real-time propagation demonstrates the dynamical stability of the condensate.

5. Summary

We have presented efficient OpenMP FORTRAN programs for solving the GP equation for a three-component spin-1 spinor BEC and used these to calculate the densities and energies for various values of system parameters. Different SO and Rabi coupling terms can be included in the programs. We provide two sets of programs: one for a quasi-1D BEC and the other for a quasi-2D BEC. Each of these programs is capable of executing both the imaginary- and the real-time propagation. The imaginary-time propagation programs yield appropriate results in agreement with variational approximation in all cases [21,30]. We use the split-step Crank-Nicolson discretization to implement time propagation, relying on our earlier OpenMP FORTRAN programs of Ref. [6]. The GP equation can be solved by imaginary- or real-time propagation with an analytic wave function or a pre-calculated numerical wave function as the initial state. We stress that the convergence with one initial state could be much faster than with another initial state, and tailoring the input wave function using an analytic or a previously calculated numerical wave function is always an advantage. We have also presented the results for density and energy of different states and compared these with analytic variational and TF approximate results.

Declaration of competing interest

The authors declare that they have no known competing financial interests or personal relationships that could have appeared to influence the work reported in this paper.

Acknowledgments

Appendix A. Detailed numerical procedure

All terms in Eqs. (1) and (2), except the last terms containing explicit complex conjugation, have the form of a conventional diagonal GP equation for a three-component BEC, whose solution procedure employing the split-step method is well known. The last non-diagonal terms in Eqs. (1) and (2), as well as the Rabi coupling terms proportional to $\widetilde{\Omega}$ require special attention. In explicit matrix notation, the split-step equation that takes into account the last terms of Eqs. (1) and (2), together with the Rabi coupling terms proportional to $\widetilde{\Omega}$, can be written as

$$i\partial_t \begin{pmatrix} \psi_{+1}(\mathbf{r}, t) \\ \psi_0(\mathbf{r}, t) \\ \psi_{-1}(\mathbf{r}, t) \end{pmatrix} = \mathbf{A} \begin{pmatrix} \psi_{+1}(\mathbf{r}, t) \\ \psi_0(\mathbf{r}, t) \\ \psi_{-1}(\mathbf{r}, t) \end{pmatrix}, \quad \text{where} \quad \mathbf{A} = \begin{pmatrix} 0 & a & 0 \\ a^* & 0 & b \\ 0 & b^* & 0 \end{pmatrix}, \tag{A.1}$$

and $a = c_2\psi_-^*\psi_0 + \widetilde{\Omega}$, $b = c_2\psi_0^*\psi_+ + \widetilde{\Omega}$. The real eigenvalues of the Hermitian matrix $\mathbf{A}$ are $\lambda_1 = C = \sqrt{|a|^2 + |b|^2}$, $\lambda_2 = 0$, and $\lambda_3 = -C$, while the corresponding eigenvectors are $v_1 = (v_{11}, v_{12}, v_{13})^T = (a, C, b^*)^T$, $v_2 = (v_{21}, v_{22}, v_{23})^T = (b, 0, -a^*)^T$, and $v_3 = (v_{31}, v_{32}, v_{33})^T = (a, -C, b^*)^T$, respectively. For a sufficiently small time step Δ, the solution of Eq. (A.1) is given by

$$\begin{pmatrix} \psi_{+1}(\mathbf{r}, t + \Delta) \\ \psi_0(\mathbf{r}, t + \Delta) \\ \psi_{-1}(\mathbf{r}, t + \Delta) \end{pmatrix} = \mathbf{V} \begin{pmatrix} e^{-i\Delta\lambda_1} & 0 & 0 \\ 0 & e^{-i\Delta\lambda_2} & 0 \\ 0 & 0 & e^{-i\Delta\lambda_3} \end{pmatrix} \mathbf{V}^{-1} \begin{pmatrix} \psi_{+1}(\mathbf{r}, t) \\ \psi_0(\mathbf{r}, t) \\ \psi_{-1}(\mathbf{r}, t) \end{pmatrix}, \tag{A.2}$$

where

$$\mathbf{V} \equiv \begin{pmatrix} v_{11} & v_{21} & v_{31} \\ v_{12} & v_{22} & v_{32} \\ v_{13} & v_{23} & v_{33} \end{pmatrix} = \begin{pmatrix} a & b & a \\ C & 0 & -C \\ b^* & -a^* & b^* \end{pmatrix}, \quad \mathbf{V}^{-1} = \frac{1}{2C^2} \begin{pmatrix} a^* & C & b \\ 2b^* & 0 & -2a \\ a^* & -C & b \end{pmatrix}. \tag{A.3}$$

In Eq. (A.2) the right-hand-side is considered known, since it is expressed in terms of the wave-function values at time t, and thus the wave function is easily propagated to time $t + \Delta$. In case of larger spins, if the matrix $\mathbf{A}$ of larger dimension cannot be analytically diagonalized, it can be diagonalized numerically by one of the many available subroutine packages.

When we consider the SO coupling terms proportional to $\widetilde{\gamma}$, they can be also evaluated at time t using the known wave-function values, and the corresponding split-step equations can be solved to propagate the wave functions to time $t + \Delta$. For example, in case of the $\gamma p_x \Sigma_x$ coupling in 1D, these are performed via

$$\psi_{\pm 1}(\mathbf{r}, t + \Delta) = \psi_{\pm 1}(\mathbf{r}, t) - \Delta\widetilde{\gamma}\partial_x\psi_0(\mathbf{r}, t), \tag{A.4}$$

$$\psi_0(\mathbf{r}, t + \Delta) = \psi_0(\mathbf{r}, t) - \Delta\widetilde{\gamma}\Big[\partial_x\psi_{+1}(\mathbf{r}, t) + \partial_x\psi_{-1}(\mathbf{r}, t)\Big]. \tag{A.5}$$

In Eqs. (A.4) and (A.5) the right-hand-side at time t is known and hence the wave-function values at time $t + \Delta$ can be obtained from those at time t. All SO coupling terms are treated in the same fashion.

The simultaneous maintenance of the normalization and magnetization m, viz. Eq. (4), during the time propagation, given by Eqs. (4), is done following the procedure of Ref. [31], by rescaling the wave-function components after each time step Δ according to $\psi_j \rightarrow d_j\psi_j$, where

$$d_0 = \frac{\sqrt{1 - m^2}}{\sqrt{N_0 + \sqrt{4(1 - m^2)N_{+1}N_{-1} + m^2N_0^2}}}, \quad d_1 = \frac{\sqrt{1 + m - d_0^2N_0}}{\sqrt{2N_{+1}}}, \quad d_{-1} = \frac{\sqrt{1 - m - d_0^2N_0}}{\sqrt{2N_{-1}}}, \tag{A.6}$$

and $N_j = \int d\mathbf{r}\, \rho_j(\mathbf{r}, t)$. However, when the SO coupling does not commute with Σ_z, we do not impose the condition of conservation of magnetization and the rescaling is done according to

$$d_0 = d_{+1} = d_{-1} = \frac{1}{\sqrt{N_0 + N_{+1} + N_{-1}}}. \tag{A.7}$$

Appendix B. Supplementary data

Supplementary material related to this article can be found online at https://doi.org/10.1016/j.cpc.2020.107657. It contains analytic variational and Thomas-Fermi approximations developed for the calculations presented in this paper.

References

[1] P. Muruganandam, S.K. Adhikari, Comput. Phys. Comm. 180 (2009) 1888.
[2] D. Vudragović, I. Vidanović, A. Balaž, P. Muruganandam, S.K. Adhikari, Comput. Phys. Comm. 183 (2012) 2021.
[3] R. Kishor Kumar, L.E. Young-S, D. Vudragović, A. Balaž, P. Muruganandam, S.K. Adhikari, Comput. Phys. Comm. 195 (2015) 117.
[4] R.K. Kumar, V. Lončar, P. Muruganandam, S.K. Adhikari, A. Balaž, Comput. Phys. Comm. 240 (2019) 74.

[5] L.E. Young-S, D. Vudragović, P. Muruganandam, S.K. Adhikari, A. Balaž, Comput. Phys. Comm. 204 (2016) 209.
[6] L.E. Young-S, P. Muruganandam, S.K. Adhikari, V. Lončar, D. Vudragović, A. Balaž, Comput. Phys. Comm. 220 (2017) 503.
[7] V. Lončar, A. Balaž, A. Bogojević, S. Škrbić, P. Muruganandam, S.K. Adhikari, Comput. Phys. Comm. 200 (2016) 406.
[8] V. Lončar, L.E. Young-S, P. Škrbić, S.K. Adhikari, A. Balaž, Comput. Phys. Comm. 209 (2016) 190.
[9] B. Satarić, V. Slavnić, A. Belić, A. Balaž, P. Muruganandam, S.K. Adhikari, Comput. Phys. Comm. 200 (2016) 411.
[10] D.M. Stamper-Kurn, M.R. Andrews, A.P. Chikkatur, S. Inouye, H.-J. Miesner, J. Stenger, W. Ketterle, Phys. Rev. Lett. 80 (1998) 2027.
[11] J. Stenger, S. Inouye, D.M. Stamper-Kurn, H.-J. Miesner, A.P. Chikkatur, W. Ketterle, Nature 396 (1998) 345.
[12] Y.-J. Lin, K. Jiménez-García, I.B. Spielman, Nature 471 (2011) 83.
[13] V. Galitski, I.B. Spielman, Nature 494 (2013) 49.
[14] D. Campbell, R. Price, A. Putra, A. Valdés-Curiel, D. Trypogeorgos, I.B. Spielman, Nature Commun. 7 (2016) 10897.
[15] L. Salasnich, A. Parola, L. Reatto, Phys. Rev. A 65 (2002) 043614.
[16] J. Dalibard, F. Gerbier, G. Juzeliūnas, P. Öhberg, Rev. Modern Phys. 83 (2011) 1523.
[17] Y. Li, Giovanni I. Martone, S. Stringari, Ann. Rev. Cold At. Mol., Vol. 3, World Scientific, 2015, p. 201 (Ch 5).
[18] Y. Kawaguchi, M. Ueda, Phys. Rep. 520 (2012) 253.
[19] V.I. Yukalov, Laser Phys. 28 (2018) 053001.
[20] S. Gautam, S.K. Adhikari, Phys. Rev. A 92 (2015) 023616.
[21] S. Gautam, S.K. Adhikari, Laser Phys. Lett. 12 (2015) 045501.
[22] S.K. Adhikari, Physica E 118 (2020) 113892.
[23] E.I. Rashba, Fiz. Tverd. Tela 2 (1960) 1224;   Sov. Phys. Solid State 2 (1960) 1109, English Transla..
[24] G. Dresselhaus, Phys. Rev. 100 (1955) 580.
[25] W. Bao, F.Y. Lim, SIAM J. Sci. Comput. 30 (2008) 1925.
[26] T. Mizushima, K. Machida, T. Kita, Phys. Rev. A 66 (2002) 053610.
[27] E.G.M. van Kempen, S.J.J.M.F. Kokkelmans, D.J. Heinzen, B.J. Verhaar, Phys. Rev. Lett. 88 (2002) 093201.
[28] A. Crubellier, O. Dulieu, F. Masnou-Seeuws, M. Elbs, H. Knöckel, E. Tiemann, Eur. Phys. J. D 6 (1999) 211.
[29] P. Schuck, X. Viñas, Phys. Rev. A 61 (2000) 043603.
[30] S. Gautam, S.K. Adhikari, Phys. Rev. A 95 (2017) 013608.
[31] F.Y. Lim, W. Bao, Phys. Rev. E 78 (2008) 066704.

Supplementary Material: Spin-1 spin-orbit- and Rabi-coupled Bose-Einstein condensate solver

1. Variational and Thomas-Fermi approximations

The Gross-Pitaevskii equations (1) and (2) can be derived from the energy functional [1, 2]

$$
\begin{aligned}
E[\psi] =\frac{1}{2} \int d\mathbf{r} \Bigg\{ & \sum_j |\nabla_\mathbf{r} \psi_j|^2 + 2V(\mathbf{r})\rho + c_0\rho^2 \\
& + c_2 \left[\rho_{+1}^2 + \rho_{-1}^2 + 2\left(\rho_{+1}\rho_0 + \rho_{-1}\rho_0 - \rho_{+1}\rho_{-1} + \psi_{-1}^*\psi_0^2\psi_{+1}^* + \psi_{-1}\psi_0^{*2}\psi_{+1} \right) \right] \\
& + \frac{\Omega}{\sqrt{2}} \left[(\psi_{+1}^* + \psi_{-1}^*)\psi_0 + \psi_0^*(\psi_{+1} + \psi_{-1}) \right] + \gamma\psi_{+1}^* f_{+1}(\partial_\mathbf{r}\psi_j) + \psi_{-1}^* f_{-1}(\partial_\mathbf{r}\psi_j) + \psi_0^* g(\partial_\mathbf{r}\psi_j) \Bigg\}.
\end{aligned}
\tag{1}
$$

We describe now two approximation schemes for the solution of the spinor GP equations, i.e., the variational approximation and the TF approximation [3, 4]. For a ferromagnetic BEC ($c_2 < 0$) without SO coupling, the ground-state densities are essentially proportional to each other, such that

$$
\psi_j(\mathbf{r}) = \alpha_j \widetilde{\psi}(\mathbf{r}), \; j = \pm 1, 0,
\tag{2}
$$

where α_j are complex numbers and the function $\widetilde{\psi}(\mathbf{r})$ is to be determined. If we substitute Eq. (2) into Eqs. (1) and (2), we obtain three equations for the unknown function $\widetilde{\psi}(\mathbf{r})$. For these equations to be consistent, one must have [3]

$$
\mu\widetilde{\psi}(\mathbf{r}) = \left[-\frac{1}{2}\nabla^2 + V(\mathbf{r}) + g\widetilde{\rho}(\mathbf{r}) \right] \widetilde{\psi}(\mathbf{r}), \quad \widetilde{\rho}(\mathbf{r}) = |\widetilde{\psi}(\mathbf{r})|^2,
\tag{3}
$$

with $g = (c_0 + c_2)$ and subject to $\int \widetilde{\rho}(\mathbf{r})\, d\mathbf{r} = 1$, with μ the chemical potential and $|\alpha_{\pm 1}| = (1 \pm m)/2$, $|\alpha_0| = \sqrt{(1 - m^2)/2}$. For the ground state of an anti-ferromagnetic BEC ($c_2 > 0$), the $j = 0$ component is absent, $\psi_0 = 0$. In this case Eq. (2) holds only for $m = 0$, with $|\alpha_{\pm 1}| = 1/\sqrt{2}, \alpha_0 = 0$, while Eq. (3) is again valid with $g = c_0$.

1.1. Variational approximation

Equation (3) can be derived by a minimization of the energy functional

$$
E = \frac{1}{2} \int d\mathbf{r} \left[\left|\nabla\widetilde{\psi}(\mathbf{r})\right|^2 + \mathbf{r}^2 \left|\widetilde{\psi}(\mathbf{r})\right|^2 + g\left|\widetilde{\psi}(\mathbf{r})\right|^4 \right].
\tag{4}
$$

We consider the variational ansatz $\widetilde{\psi}(\mathbf{r}) = \left[w\sqrt{\pi} \right]^{-d/2} \exp\left(-\frac{\mathbf{r}^2}{2w^2}\right)$ where $d = 1$ in 1D and $d = 2$ in 2D, and w is a variational parameter. With this ansatz the energy functional becomes

$$
E = \frac{d}{4w^2} + \frac{dw^2}{4} + \frac{g}{2\left(w\sqrt{2\pi} \right)^d}.
\tag{5}
$$

The parameter w is obtained by a minimization of this energy.

1.2. Thomas-Fermi approximation

In absence of SO coupling ($\gamma = 0$), for an anti-ferromagnetic ($c_2 > 0$) spin-1 BEC with zero magnetization and for a ferromagnetic ($c_2 < 0$) spin-1 BEC, there are simple analytic solutions based on a decoupled mode TF approximation and we quote the results here. The density of the three components are given by [3]

$$\rho_j(\mathbf{r}) = |\alpha_j|^2 \rho_{\text{TF}}(\mathbf{r}) = |\alpha_j|^2 \frac{L_d^2 - \mathbf{r}^2}{2g} \tag{6}$$

where $L_1 = [3g/2]^{1/3}$ in 1D and $L_2 = [4g/\pi]^{1/4}$ in 2D. In 1D this density is the linear density, while in 2D it is the radial density. The TF energy can be evaluated and yield $E_{\text{TF}} = 3[3g/2]^{2/3}/10$ in 1D, and $E_{\text{TF}} = 2\sqrt{g/\pi}/3$ in 2D.

Some useful analytic results can be obtained for a ferromagnetic BEC in 1D in the absence of magnetization ($m = 0$) for non-zero SO ($\gamma \neq 0$) and Rabi ($\Omega \neq 0$) coupling strengths. The ansatz for the wave function components is taken to be $\alpha_{\pm 1} = e^{i\gamma x}/2, \alpha_0 = -e^{i\gamma x}/\sqrt{2}$ in Eq. (2), viz. Eq. (22) of Ref. [5]. For the SO coupling of the form $\gamma p_x \Sigma_x$, the total energy for small values of $\gamma \neq 0$ can be now evaluated to yield $\widetilde{E}_{\text{TF}} = E_{\text{TF}} - \frac{\gamma^2}{2} - \Omega$, where E_{TF} are the above calculated expressions in 1D or 2D. In this case the TF profile for the density remains unchanged for small γ and Ω. However, the energy gets modified due to the SO and Rabi couplings.

Additional useful analytic results can be obtained for an anti-ferromagnetic BEC in 1D in the absence of magnetization ($m = 0$) for a non-zero SO coupling strength ($\gamma \neq 0$). The ansatz for the wave function components in this case is taken to be $\alpha_{\pm 1} = i\sin(\gamma x)/\sqrt{2}, \alpha_0 = -\cos(\gamma x)$ in Eq. (2), viz. Eq. (18) of Ref. [5]. For the SO coupling of the form $\gamma p_x \Sigma_x$, the total TF energy for small values of $\gamma \neq 0$ and $\Omega \neq 0$ can be now evaluated: $\widetilde{E}_{\text{TF}} = E_{\text{TF}} - \frac{\gamma^2}{2}$. The TF profile for the density remains unchanged for small γ, but the energy gets modified due to the SO coupling.

References

[1] Y. Kawaguchi, M. Ueda, Phys. Rep. 520 (2012) 253.
[2] V. I. Yukalov, Laser Phys. 28 (2018) 053001.
[3] S. Gautam, S. K. Adhikari, Phys. Rev. A 92 (2015) 023616.
[4] P. Schuck, X. Viñas, Phys. Rev. A 61 (2000) 043603.
[5] S. Gautam, S. K. Adhikari, Laser Phys. Lett. 12 (2015) 045501.

What Information on Volatile Organic Compounds Can Be Obtained from the Data of a Single Measurement Site Through the Use of Artificial Intelligence?

Svetlana Stanišić, Mirjana Perišić, Gordana Jovanović, Dimitrije Maletić, Dušan Vudragović, Ana Vranić, and Andreja Stojić

Abstract Increasing air pollutant concentrations over the last few decades have been a focus of contemporary scientific research due to adverse effects on public health, the environment and climate change. In this chapter, we used an innovative integrated methodology for spatio-temporal characterization of sources and concentration forecasts of toxic, mutagenic and carcinogenic representatives of volatile organic species—benzene, toluene, ethylbenzene and xylene, commonly referred to as BTEX. The methodology is based on receptor-oriented air circulation modeling and artificial intelligence implemented through machine learning and explainable artificial intelligence methods. The study covered two years of data obtained from a single monitoring station located at 54a Despota Stefana Boulevard (44°49'68" N, 20°28'04" E). This station was selected from the local and state network for air quality monitoring in the territory of Belgrade. The receptor-oriented modeling was effective for classifying sources of BTEX and the assessment of BTEX concentra-

S. Stanišić (✉)
Environment and Sustainable Development, Singidunum University, Belgrade, Serbia
e-mail: sstanisic@singidunum.ac.rs

M. Perišić · G. Jovanović · D. Maletić · D. Vudragović · A. Vranić · A. Stojić
Institute of Physics Belgrade, National Institute of the Republic of Serbia, Environment and Sustainable Development, Singidunum University, Belgrade, Serbia
e-mail: mirjana.perisic@ipb.ac.rs

G. Jovanović
e-mail: gordana.vukovic@ipb.ac.rs

D. Maletić
e-mail: dimitrije.maletic@ipb.ac.rs

D. Vudragović
e-mail: dusan.vudragovic@ipb.ac.rs

A. Vranić
e-mail: ana.vranic@ipb.ac.rs

A. Stojić
e-mail: andreja.stojic@ipb.ac.rs

tions in the Belgrade urban area surrounding the receptor site that was not regularly monitored. The correlations and ratios between BTEX compounds were used for estimating their interrelationships and presence in the air, which contributed to the identification of their origin. Also, this study evaluated the possibilities of BTEX spatio-temporal forecasts based on the integrated methodology. For this purpose, XGBoost was efficient at forecasting BTEX levels, with estimated errors (6–15%) significantly below the uncertainty obtained by conventional models for the evaluation of average annual pollutant concentrations. The results suggest that temperature, wind speed and wind direction represented the main parameters which explain the spatio-temporal distribution of BTEX, while the impact of other factors showed significant variations depending on the locations of the receptor and the compound.

1 Introduction

Growing urban populations, economic development, and transport have a significant impact on environmental pollution. Air pollution constitutes a major underestimated cause of non-communicable diseases, being responsible for 19% of all cardiovascular deaths and 23% of lung cancer deaths globally [19]. Around 91% of the world's population lives in areas where air pollution levels exceed the World Health Organization's recommended values [43]. People often perceive air pollution as an issue that affects people living in middle- and low- income countries or people living in megacities. However, it has been estimated that out of 8.8 million global deaths associated with air pollution in 2015, 8% were citizens of high-income countries, mostly those living in small urban areas where the topography and climate contribute to high air pollutant concentrations [3, 7]. Holgate [17] emphasizes that annually, 40,000 excess deaths in the UK can be attributed to low air quality. Society might be much more aware of this issue if the mortality was a result of drinking polluted water. Air pollution in households has decreased since the 1990's as new fuels such as petroleum gas and renewable sources of energy have replaced biomass. In developing countries, residential combustion of solid fuels for cooking and heating remains a significant source of air pollution and a major concern due to its detrimental health effects, particularly in rural areas [9]. In contrast, in developed countries, indoor air pollution is less important because adverse health effects are associated with exposure to outdoor pollutant concentrations that have decreased over previous decades. However, it has also been estimated that the rapid expansion of metropolises, industrial production, increasing pesticide use, toxic chemicals and motor vehicles will offset the effects of air pollution mitigation measures [13].

Among the air pollutants that are of interest for current and future research due to their detrimental effects on both human health and the environment are volatile organic compounds (VOCs). VOCs are a heterogeneous group of organic species

with boiling points $<250\,°C$. Their representatives are benzene and its alkylated derivatives toluene, ethylbenzene and xylene, commonly referred to as BTEX. Over the last few decades in developed countries, reducing BTEX levels has been a challenge [26]. This is due to their abundance, their numerous emission sources, their complex atmospheric chemistry, insufficient funds for the establishment and maintenance of monitoring networks, and the fact that abatement programs might have negative impacts on economic output because they are among the most abundantly produced compounds worldwide. They are used as feedstock for several materials and products upon which modern society has become dependent. These compounds are naturally found in crude oil, while in urban and suburban areas they originate from traffic emissions, commercial and industrial uses of petroleum, gasoline, adhesives, coatings, degreasers, solvents, detergents, explosives, pesticides, resins, ink, paints, and varnishes [30, 33, 35]. With the exception of m-/p-xylene, concentrations of BTEX were mostly reported to be higher in indoor air than outdoor air [4].

The health effects of BTEX are wide-ranging. Studies have shown that BTEX can be found in cord blood and the blood of children and adults, particularly adults that are occupationally exposed [18]. Research has shown that long-term exposure to high benzene concentrations increases the risk of developing malignant blood disorders, while long-term exposure to high toluene concentrations causes renal tubular acidosis [42]. Some studies have shown that after benzene concentrations in industrial and urban areas are reduced, lifetime cancer risk decreases by one order of magnitude [20]. In addition, exposure to ambient levels of BTEX, which in many cases were orders of magnitude below the reference concentrations, can be dangerous. This is particularly true during the susceptibility period when exposure can lead to the disruption of endocrine signaling (which is essential for the growth and development), immune responses, reproduction, cardiovascular function and aging. Therefore, populations in highly industrialized areas, the socioeconomically deprived, as well as children, pregnant women and elderly people, appear to be more susceptible to pollution-related morbidity and mortality [5, 32]. While traffic emissions are known to be the main source of outdoor BTEX, converting to alternative renewable energy sources will not reduce demand for consumer products, and the replacement of benzene with safer alternatives, such as toluene and xylene, might ultimately be a poor solution once long-term toluene and xylene exposure scenarios are considered [4]. According to a United States Environmental Protection Agency [40] report, ethylbenzene is sixth on a list of the top 20 chemicals used in children's products, primarily food packaging, toys, sport equipment, arts, crafts and hobby materials. Toluene, on the other hand, is the seventh most used chemical in consumer products, primarily fuels, paints, and coatings. Although toluene and xylenes are less harmful than benzene, it should be kept in mind that the products of photochemical reactions in which BTEX are involved often have more harmful effects on human health than their precursors [14]. It should be also mentioned that limited ventilation in closed premises can often be the reason why indoor BTEX levels are higher than outdoor levels [29].

Apart from their impacts on human health, BTEX and other VOCs are associated with increases in the oxidation capacity of the atmosphere, as well as with the

generation of secondary pollutants, such as tropospheric ozone, polycyclic aromatic hydrocarbons and secondary aerosol through photochemical reactions [8, 36]. As regards the impact on global warming, not only do volatile species directly and indirectly contribute to climate change, but their emission and fate are expected to be influenced and increased by global warming.

Despite vast changes in the development and integration of different approaches in the field of environmental science, spatio-temporal air pollution modeling remains a challenge. Two main approaches are typically utilized to forecast air quality and to identify the factors that govern the concentrations of certain pollutants. The first approach relies on atmospheric diffusion models, while the second refers to statistical models that capture the essential relationships between the variables [24]. Multidimensionality and the size of data sets, as well as the complexity of air pollutant processes and interactions, set requirements that exceed the capabilities of conventional statistical methods. For this reason, machine learning (ML) methods and explainable artificial intelligence (XAI), subfields of artificial intelligence (AI) that enable automatized big data analysis and the development of learning algorithms, have been introduced into environmental science research. In this paper, we used an innovative and integrated methodology based on artificial intelligence and implemented through ML ana XAI methods for the modeling of spatio-temporal air pollution and the characterization of BTEX sources in a wider region surrounding the receptor site that was not covered by regular monitoring. The obtained BTEX correlations and ratios were used for estimating the interrelationships between the species in the air, while XGBoost was utilized for efficient spatio-temporal BTEX forecasting. The present paper is an extended version of the study presented at the International Scientific Conference on Information Technology and Data Related Research (Sinteza 2020), Singidunum University [38].

2 Materials and Methods

Nowadays, there are a large number of libraries implemented in different programming languages (R, Python, JS) that deal with interactive display (plotly, leaflet) and spatial data analysis. In addition to various spatial autocorrelation possibilities, the analysis of spatial data patterns, the interpolation of data by statistical methods such as Kriging, Spline or Inverse Distance Weighting, and machine learning methods such as Random Forests are increasingly used. Furthermore, spatial distributions of air pollutant sources can be estimated using general and local hybrid receptors, as well as by analyzing clustered data [9, 33, 34].

Significant improvements to the general hybrid receptor modeling approach have been made in recent decades. Receptor-oriented methods, based on conditional probability and analyzing the residence time of pollutants in an area, have become widely accepted both for studying the dynamic processes and circulation patterns of pollutants in the atmosphere and for investigating the spatial distribution of potential

emission sources and their impact on the receptor site without relying on an emission inventory.

The identification of potential emission sources at a local level, as well as their contribution to the measured concentrations of pollutants at the receptor site, can be determined by models analogous to the general hybrid receptor model such as the Potential Source Contribution Function (PSCF), Concentration-Weighted Trajectories (CWT), sQTBA (Simplified Quantitative Transport Bias Analysis) and RTWC (Residence Time Weighted Concentration). The general models, which are based on the analysis of trajectory end points, can be improved by using local wind parameters. This way it is possible to determine pollution circulation patterns very accurately in the area around a given measuring point. A local three-dimensional hybrid receptor model similar to the 3D CWT model was developed for the purposes of this paper [34]. The study involved two-years of regular measurements of BTEX, suspended particles, inorganic gaseous oxides, and meteorological parameters within the Belgrade City Institute for Public Health's automatic monitoring network (44°49'68" N, 20°28'04" E).

Machine learning is an area of artificial intelligence that involves the development of algorithms that can learn based on input data and can thus be trained to predict value variations. Machine learning algorithms are based on the extraction of patterns and the selection of specific attributes from a large number of data, while eliminating irrelevant information. Through identifying most important prediction attributes, machine learning methods acquire knowledge and define the substantial relationships that exist between input and output parameters by focusing on the aspect of the data that is the most useful for efficient forecasting.

Forecasting the concentration dynamics of BTEX in the air was done using the Xtreme Gradient Boosting (XGBoost) method [11], with meteorological data used as predictors. XGBoost is a general-purpose ensemble method of supervised machine learning which combines the results of many decision trees and achieves high accuracy in a wide range of practical applications. It usually outperforms support vector machines, random forests, and deep learning neural networks [31]. The main advantage of the XGBoost method is its obtainment of more precise predictions than those provided by single constitutive decision algorithms. XGBoost is based on a boosting technique that sequentially defines a series of decision trees for classifying input data into two or more attribute-defined classes. Each consecutive decision tree is trained through iterations, taking into account the previously registered classification errors. The datasets from each of the grid cells used for spatio-temporal BTEX forecasting was split into training (80%) and validation (20%) sets. Hyperparameter tuning was implemented using a brute-force grid search and a 10-fold stratified cross-validation. The best performing hyperparameter values were used in the final model.

Methods based on decision trees, such as Gradient Boosting and Random Forests, have been shown to provide inconsistent attribute contributions. This has led to the development of SHAP (SHapley Additive exPlanation), a method that estimates the contribution of each instance of an attribute, which enables interpretation of the model's outputs [15, 21, 31]. To explain the contribution of each feature to the individual XGBoost prediction, the SHAP method was utilized [21]. It is based on

coalitional game theory and provides a distribution of each prediction among the features represented as additive attributions. In this study, we used Python SHAP implementation (SHAP Python package). The captured importance of a feature is visually presented as a SHAP summary plot.

3   Results and Discussion

Previous studies have demonstrated strong gradients and pronounced intra-urban spatial variability of pollutant levels. This depends on traffic density, street configuration and prevailing wind direction [41]. In addition to this, Ning et al. [27] emphasized the importance of terrain complexity for air quality because topographic features can, to a certain extent, limit pollutant dispersion under different weather conditions. The results indicate that BTEX concentrations were significantly higher in areas with dense traffic, in the vicinity of busy streets and intersections, where traffic emission sources have a high impact, where local topography limits natural ventilation and vertical dispersion of pollution, and in areas with narrow streets lined by tall buildings and trees.

3.1   *BTEX Levels Surrounding the Receptor Site*

Benzene concentrations were estimated to range from 1.2 to 2.6 $\mu g\,m^{-3}$, with an average level of 2.6 $\mu g\,m^{-3}$. In a few locations, estimates of pollutant concentrations were extremely high, exceeding the recommended limit of 5 $\mu g\,m^{-3}$. Extreme benzene levels in areas distant from the receptor site should be taken with caution. This is due to a relatively small number of events and therefore limited data produces the calculated values. It has been estimated that the area surrounding the receptor site was mostly influenced by traffic emissions. Other studies have reported that similar average benzene concentrations are sometimes discovered in urban areas where traffic is the predominant source of pollutant emissions [2]. Concentrations of toluene were estimated to range from 0.9 to 8.9 $\mu g\,m^{-3}$ with an average value of 8.7 $\mu g\,m^{-3}$, while the average m/p-xylene concentrations were assessed to be several times higher (8.4 $\mu g\,m^{-3}$) than the concentrations of o-xylene (1.8 $\mu g\,m^{-3}$). Concentrations of ethylbenzene were estimated to range from 0.2 to 2.1 $\mu g\,m^{-3}$ with an average value of 1.8 $\mu g\,m^{-3}$. As predicted, TEX levels were highest in the city center and the north of the city. The assessed TEX levels were also consistent with the reported values for outdoor TEX concentrations in various studies published over the last two decades [1, 10, 16, 23, 25], with somewhat lower levels of toluene than typically expected in an urban area.

3.2 Seasonal and Daily BTEX Variations

While the intensity of BTEX emission sources tend to be higher in winter, evaporations in warmer parts of the year make an important contribution to total pollutant concentrations. On the other hand, the stability of atmospheric conditions and decrease in chemical reactivity of BTEX in winter results in longer retention in ambient air [29]. Furthermore, BTEX are known to exhibit variations on a daily basis. For instance, a previous study that contained a risk assessment of an accidental benzene release in an urban area using an atmospheric dispersion model, showed that benzene spreads over a much larger area during the nighttime due to a stable boundary layer. In contrast, enhanced vertical mixing results in limited dispersion of the pollutant over the study area during the daytime [39]. Similar results were obtained in our study.

3.3 BTEX Forecasting Based on Meteorological Variables as Predictors

As can be seen in Figs. 1 and 2, high correlation coefficients between predicted and observed values (>0,80) were obtained for most of the analyzed data, it can therefore be concluded that XGBoost was a successful and efficient method for forecasting air pollution in an urban area. It should be emphasized that the estimated method errors (6–15%) were significantly lower than the uncertainty (50%) which is required for the evaluation of average annual pollutant concentrations using conventional modeling.

It should be also emphasized that due to the relatively short atmospheric lifetimes of BTEX, the area that can be affected by BTEX emissions is approx. 15–20 km [29], but the consistency of meteorological conditions significantly affects the extent of volatile pollutant dispersion.

The results of this study suggest that low temperatures and weak to moderate wind represent the main parameters which govern the spatio-temporal distribution of benzene in a majority of locations. The impacts of other factors display significant variation depending on the characteristics of the receptor's location (Fig. 1). Namely, one can note that the horizontal axis marked with wind speed is the longest, which means that benzene concentrations were mostly affected by this parameter. Each axis is composed of a series of points that represent the measured values of the predictor. As can be seen in the example for wind speed, extremely high wind speeds, represented by points located on the far right of the axis, have relatively little impact on benzene concentrations in the air. This suggests that benzene concentrations were mostly influenced by weak to moderate wind, which further suggests that emission sources located in the vicinity of the selected receptor site have the highest impact.

Furthermore, the importance of a certain wind direction for pollutant level prediction is related to the position of the emission source which affects the receptor location the most. Namely, in cases where a single pollutant emission source has a
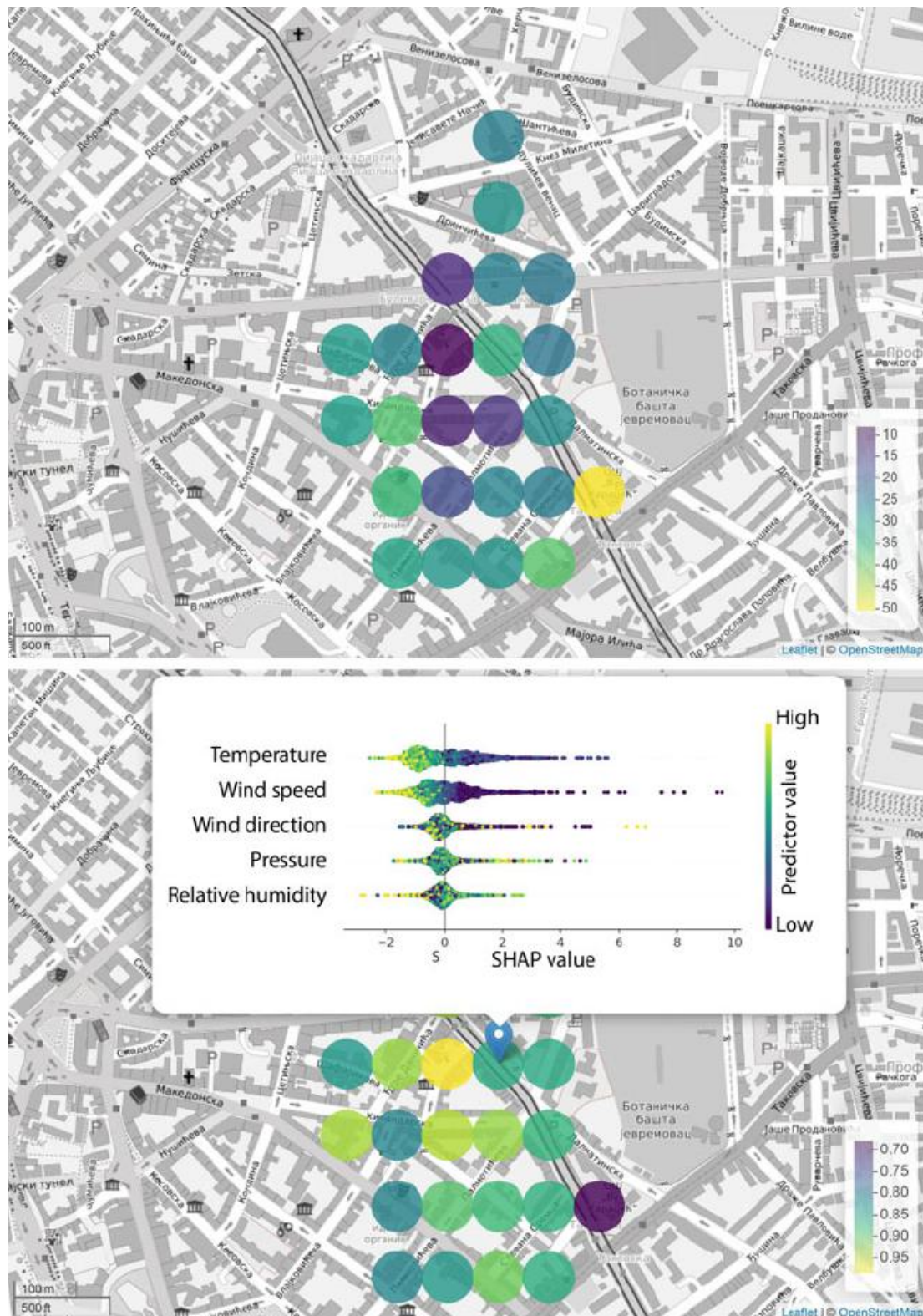
Fig. 1 Benzene forecast based on meteorological parameters—a relative error [%] (top) and SHAP values and predicted/observed correlation coefficients (bottom)
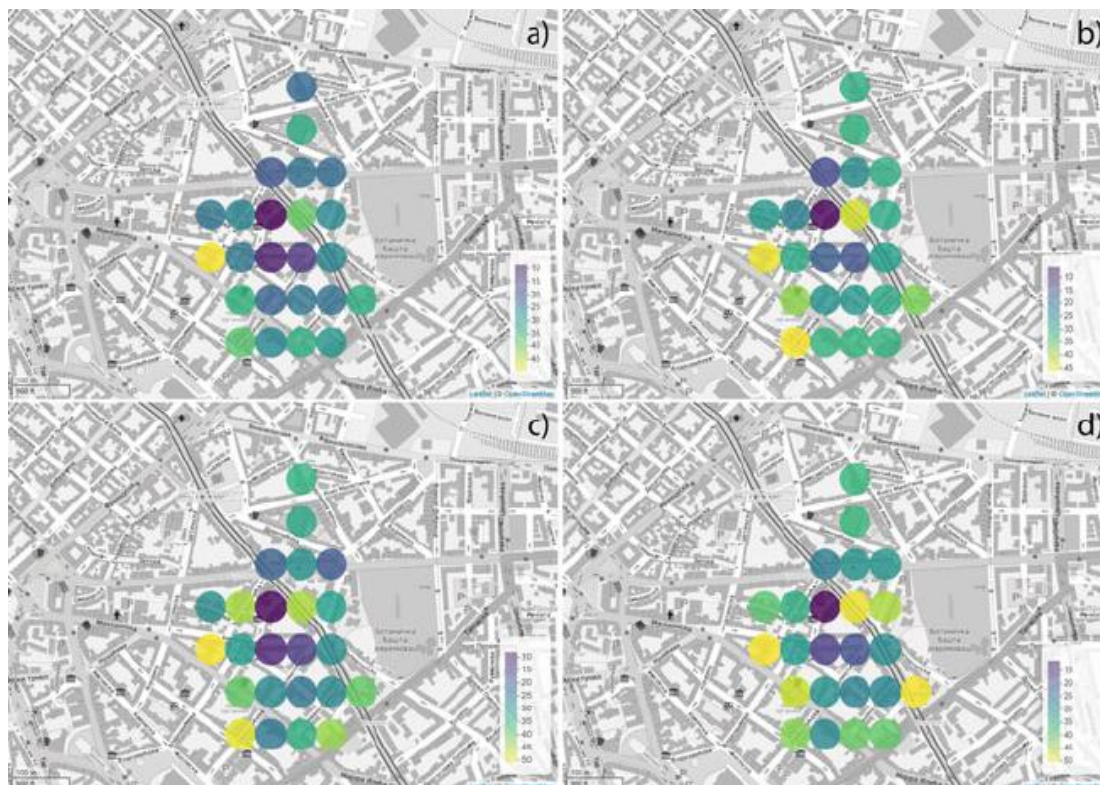
Fig. 2 Toluene (**a**), m,p-xylene (**b**), o-xylene (**c**), and ethylbenzene (**d**) relative error [%] forecasts based on meteorological parameters

major effect on the receptor area, the importance of wind direction as a predicting factor is particularly accentuated. Additionally, the importance of wind direction is evident in situations where tall buildings and trees along the roadside form a corridor that either hinders or assists polluted air masses from the surrounding emission sources, which was the case in this study as well. The importance of relative humidity as predictor for benzene concentrations was predicted to be high in the event of extreme benzene levels. This is because benzene and TEX are partially water-soluble compounds, which suggests that both high and low levels of relative humidity can impact their ambient air levels [28].

The presented figures displaying TEX distributions can be interpreted in the following manner. Atmospheric pressure and wind parameters appear to be the major predictors of TEX behavior in general. The impacts of air temperature and pressure were significantly lower for forecasting toluene levels (Fig. 2) than for forecasting benzene levels, which can be explained by the fact that benzene evaporates at significantly lower temperatures than toluene.

The correlations between the observed and forecasted concentrations of benzene ranged from 0.70 to 0.95, but most often ranged from 0.80 to 0.85. At the location where the correlation was the highest (0.95), benzene concentrations were forecasted with a relative error of 8%, while the most influential SHAP-revealed factor was wind direction. The correlations between the observed and forecasted concentrations of toluene ranged from 0.65 to 0.95, but mostly around 0.80.

At the location where the correlation was the highest (0.95), toluene concentrations were forecasted with a relative error of 9%, while the most influential SHAP-revealed factors were wind speed and direction. The correlations between the observed and forecasted concentrations of m/p-xylenes ranged from 0.65 to 0.95, but averaged approximately 0.75. At the locations where the correlations were highest (0.97 and 0.98), the concentrations of m/p-xylenes were forecasted with relative errors of 6% and 15% respectively, while the most influential SHAP-revealed factors were wind speed, direction, and air pressure. The correlation between the observed and forecasted concentrations of o-xylene ranged from 0.60 to 0.90, with an average of approximately 0.85. At the locations where the correlations were the highest (0.94 and 0.95), o-xylene concentrations were forecasted with relative errors of 12% and 8% respectively, while the most influential SHAP-revealed factors were wind direction and air pressure. The correlations between the observed and forecasted concentrations of ethylbenzene ranged from 0.60 to 0.95, but averaged approximately 0.80. At the location where the correlation was the highest (0.95), ethylbenzene concentrations were forecasted with a relative error of 11%, while the most influential SHAP-revealed factors were wind speed, wind direction, and air pressure.

Although the results demonstrate the capacity of an innovative methodology to identify the importance of certain meteorological factors as predictors of air pollutant concentrations, the fact that variations of meteorological parameters cause changes in other related parameters makes it difficult to distinguish their actual impact on air pollution phenomena. Thus, the impact of meteorological factors should not be observed as the isolated effect of a single parameter and its variations, but as the effect of a certain type of weather. For instance, Liao et al. [22] identified ten typical air circulation types within one of the most polluted areas of China and explored how their synergetic relationship with topography affected the local air quality.

3.4 The Importance of Other Pollutants as Predictors for BTEX Levels

Apart from meteorological parameters, other analyzed factors can be considered important for predicting BTEX concentrations. Namely, for forecasting benzene levels, high CO concentrations appear to be the most important (Fig. 3), with the importance of the other predictors stated here in decreasing order: toluene > ethylbenzene > m/p-xyneles > o-xylene > PM_{10} > NO_x > NO_2 > NO > SO_2.

As regards forecasting toluene levels, high m/p-xylenes, o-xylene and CO concentrations appear be the most important, with the importance of the other predictors stated here in decreasing order: ethylbenzene > benzene > PM_{10} > NO > NO_x > SO_2 > NO_2. As regards forecasting m/p-xylenes levels, high toluene, o-xylene, ethylbenzene and CO concentrations appear to be the most important, with the importance of the other predictors stated here in decreasing order: benzene > NO_2 > NO_x > PM_{10} > SO_2 > NO. As regards forecasting o-xylene levels, high m/p-
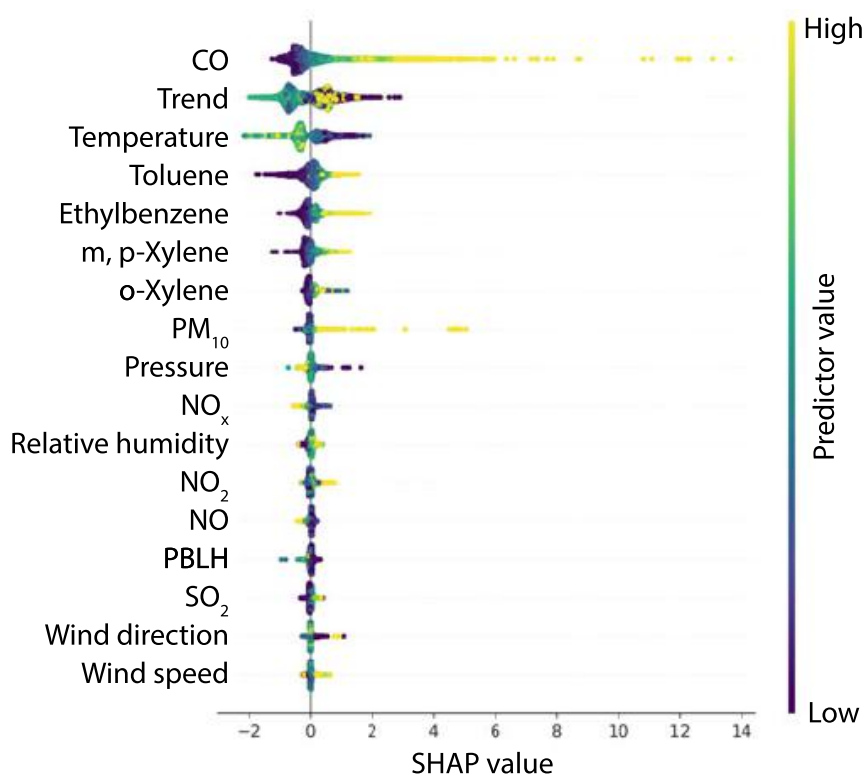
Fig. 3 SHAP summary plot for benzene

xylenes, toluene, ethylbenzene and NO concentrations appear to be the most important, with the importance of the other predictors stated here in decreasing order: NO_x > benzene > CO > PM_{10} > NO_2 > SO_2. As regards forecasting ethylbenzene levels, high m/p-xylenes, o-xylene and benzene concentrations appear to be the most important, with the importance of the other predictors stated here in decreasing order: toluene > NO_2 > SO_2 > CO > PM_{10} > NO > NO_x.

3.5 The Interdependence of BTEX Level Predictors

As part of forecasting pollutant concentrations, an examination of the interdependence between individual predicting factors and their combined effect on BTEX concentrations in the air was performed. As shown in the Fig. 4, during the cold part of the year, when temperatures were below 14 °C, concentrations of benzene are better predicted by toluene levels. Conversely, on days when the temperature exceeded 14 °C, benzene and toluene didn't share the same emission sources. Furthermore, during the cold part of the year, benzene concentrations are either significantly higher or lower than average, depending on whether the location is affected by the burning of fossil fuels for heating or not, while during the warmer part of the year benzene concentrations at different locations tended to be more uniform. This is because higher temperatures cause benzene to evaporate at all locations.
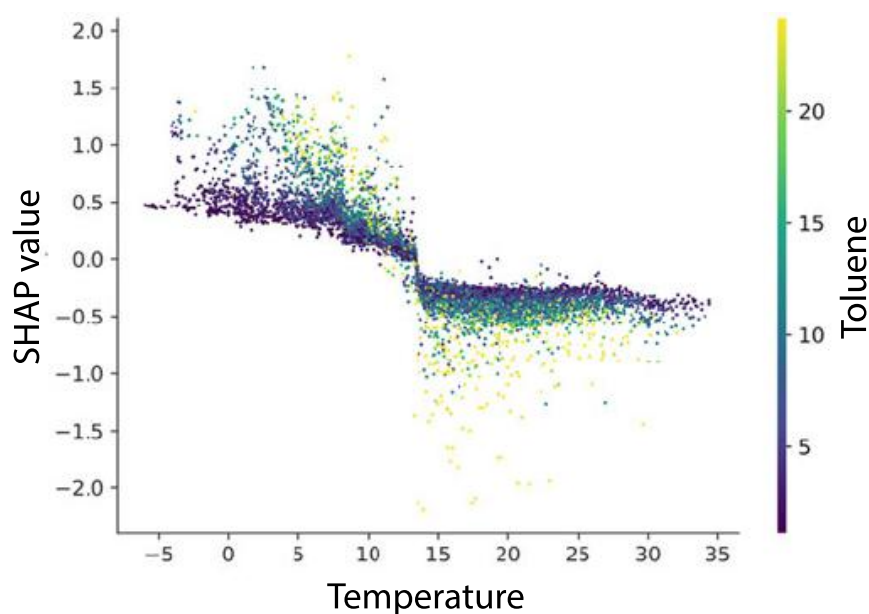
Fig. 4 Benzene SHAP dependency on temperature and toluene

In addition to temperature-toluene interactions, the results suggest that the concentrations of benzene in the ambient air depended on interactions between temperature and carbon monoxide as well. While the effects of interactions between ethylbenzene-m/p-xylenes, ethylbenzene-toluene, ethylbenzene-carbon monoxide and m/p-xylene-carbon monoxide were found to be of minor importance as regards shaping benzene concentrations (Fig. 5).

3.6   Pollutant Correlations and BTEX Origin

The results show moderate correlations between toluene and NO_x and CO concentrations throughout the city. The locations with toluene-NO_x correlations exceeding 0.7 are considered to be affected by burning-related emissions and not by toluene evaporations (Fig. 6).

Relatively high correlations between benzene and carbon monoxide were registered throughout the city, with the notable exception of the south (Fig. 7). The correlations between benzene and SO_2, NO_x and PM_{10} were lower in the eastern, and higher in the western, part of the urban region. These results suggest that benzene in the eastern area of the city is associated with evaporations and emissions from the petrochemical industry such as the Pančevo Oil refinery and the Petrohemija chemical plant. Furthermore, high correlations (r > 0,70) between benzene and inorganic oxides in the western region of the city may suggest that traffic emissions, as well as remote air pollution sources such as TPP Nikola Tesla A and B in Obrenovac, have a detrimental impact (Fig. 7). The significantly lower correlations between benzene and inorganic oxides, that can be considered indicators of combustion processes in
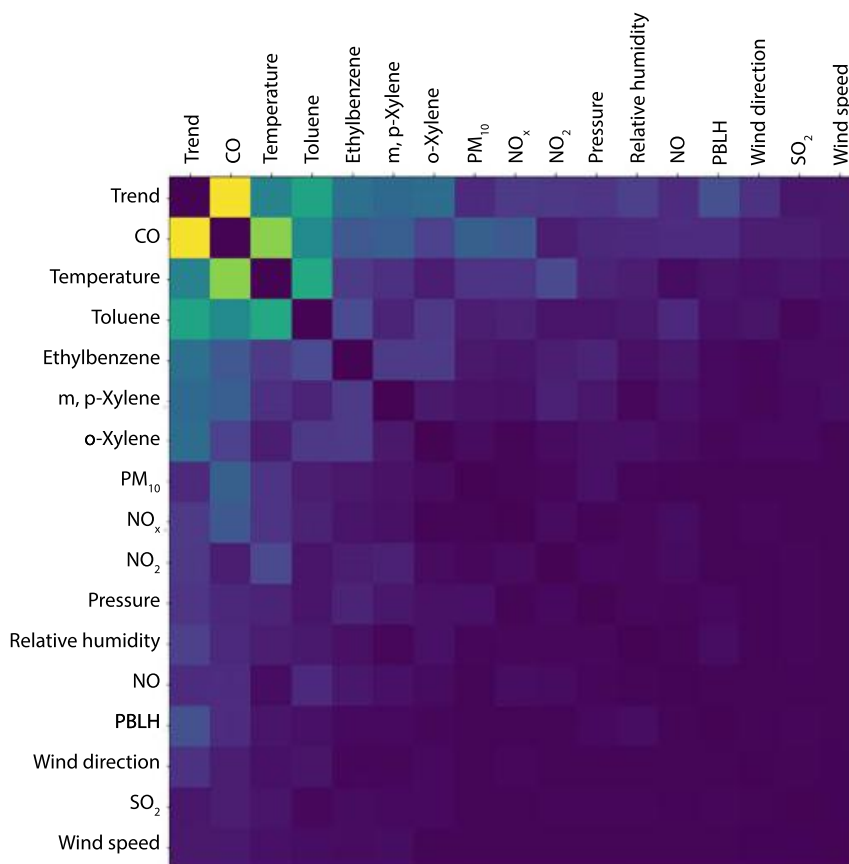
Fig. 5 SHAP interaction plot

the southern part of the city center, probably reflect the impact of gasoline evaporation. This conclusion appears more likely when we take into account that benzene concentrations were assessed to be the lowest in the southern area.

The m/p-xylenes exhibited the highest correlations with NO_x, somewhat lower correlations with CO, while the correlations with SO_2 and PM_{10} tended to be significantly lower throughout the city. A similar calculation was obtained for o-xylene and ethylbenzene.

3.7 BTEX Ratios

The benzene-to-toluene (B/T) ratio is often used as an index for identifying emission sources, while xylenes-to-benzene (X/B) and ethylbenzene-to-benzene (E/B) ratios are generally applied as indices of photochemical reactivity [12]. According to the literature, a B/T ratio below 0.5 suggests that vehicle emissions are the predominant source of BTEX, while X/B and E/B ratios below 1 suggest that sampled air masses are photochemically aged. As the results show, the B/T ratios were approx. 0.3, while the X/B and E/B ratios ranged from 0.7 to 4 with lower ratio values calculated for
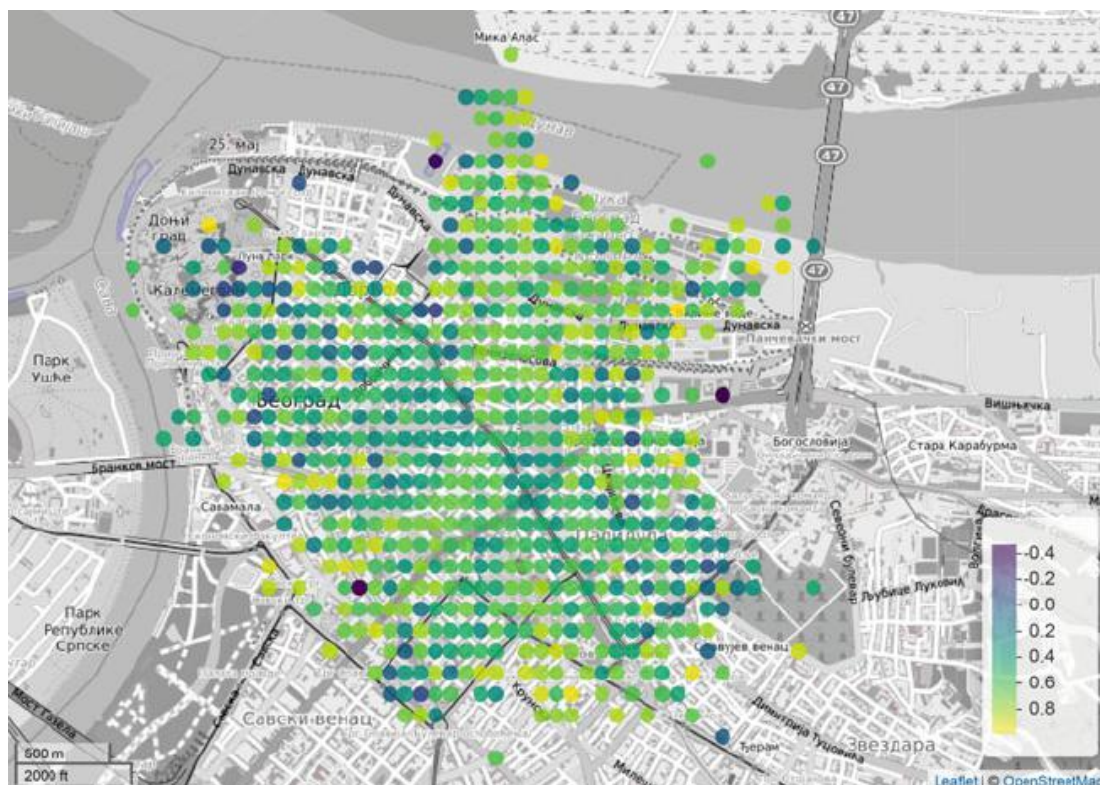
Fig. 6 Toluene and NO_x correlations

the central area of the city where narrow streets and tall buildings restrict pollutant dispersion and support the photochemical aging of the emissions. Buczynska et al. [6] showed that B/T ratios ranging from 0.22 to 0.26 for locations that were affected by traffic emissions, while the authors mentioned that ratios below 0.1 reported in previous research suggest additional emission sources of toluene, like industrial emissions, that contribute to high values. It could be concluded from the results that in most locations, BTEX concentrations in ambient air are a result of recent emissions, while traffic emissions might be the major contributor to BTEX concentrations in the analyzed area. Furthermore, BTEX have a similar chemical structure, but there is a difference in the reactivity of these typically unreactive compounds. Namely, benzene is more stable and has a longer atmospheric lifetime [14] which can significantly modify the starting BTEX concentration ratios, and thus another possibility indicated by the B/T ratio is related to aging air masses. Namely, after being emitted from a common source, toluene is about 5 times more reactive than benzene, which is why a high B/T ratio is an indicator of aged air masses. The results suggest that the examined area can be divided diagonally into two segments:

- The north-western and north-eastern area which covers the old city center where the B/T ratio is relatively high. The north-western part is subject to emissions from the industrial area, which includes the petrochemical industry comprised of the Pančevo Oil refinery and the Petrohemija chemical plant. The north-western part is subject to the retention of aged air masses in narrow streets which form an urban

Fig. 7 Benzene correlation coefficients with CO (**a**) and NO$_x$ (**b**)

canyon. The south-western part is subject to the influence of aged air masses from Obrenovac.
- The southern area, covers a large area of the city which displays a relatively low B/T ratio. This indicates the predominant effect of traffic emissions.

Although diagnostic concentration ratios are a commonly used tool for identifying and distinguishing emission sources, they should be used with caution since the calculated values often exhibit seasonal variations and can be susceptible to distortions from a number of environmental factors [37].

4 Conclusions

Identifying pollutant emission sources, investigating the temporal dynamics and spatial distributions of pollutant concentrations, and estimating the contribution of certain emission sources to local air quality are of great importance. They can help to develop an essential understanding of the impact key factors have on processes within natural and anthropogenic ecosystems and their resilience, but are also crucial for defining strategies aimed at improving air quality, resolving environmental issues, and improving human health. While soil and water pollution is mainly of local significance, air pollution can affect very remote areas given meteorological conditions that enable the transportation of pollutants. In addition to this, a number of other factors can contribute to the final effect of meteorological conditions on air pollutant concentrations, including the distribution of pollutant emission sources, local topography, street geometry and the distribution of all elements and surfaces that can be of significance for the air flow regime, pollutant dispersion conditions, their transport pathways and thus, the spatio-temporal variability of their levels. The multidimensionality of modern data, the scope of time series, as well as the complexity of processes and interactions in which air pollutants participate, are too demanding for conventional statistical methods. For this reason, recent decades have seen research conducted to find alternative methods for data analysis. One of the approaches that has proven effective in many professional and scientific fields, including environmental protection, is machine learning which provides the tools for automated analysis of a large amount of data.

As can be concluded, we have demonstrated the use of an efficient methodology for spatio-temporal BTEX concentration modeling in the Belgrade area, based on receptor-oriented air circulation modeling and artificial intelligence implemented through machine learning and explainable artificial intelligence methods. The estimated method errors ranged from 6 to 15%, which is significantly lower than the required uncertainty for conventional models. The presented methodology has the potential to provide a basis for the establishment of a unique and sustainable system for identifying sources of air pollution and enhanced air pollution data coverage that does not require additional investments in monitoring equipment. In the long term, the results of such an approach would provide a solid basis for establishing a sustain-

able system for improving the management and control of air pollution. As the results show, temperature, pressure, wind speed and wind direction were the main parameters which governed the spatio-temporal distribution of BTEX, while the impact of other factors showed significant variations depending on the characteristics of receptor's location and the compound. In addition, spatial correlations and ratios between different air pollutant concentrations were considered for determining their origin in all the locations covered by our analysis. All examples illustrate how the application of SHAP and other supplemental methods can provide a systematic insight into the impact of emission sources and environmental factors on the presence of BTEX in the air.

References

1. Abd Hamid, H., Latif, M.T., Nadzir, M.S.M., Uning, R., Khan, M.F., Kannan, N.: Ambient BTEX levels over urban, suburban and rural areas in Malaysia. Air Qual. Atmos. Health **12**, 341–351 (2019)
2. Baltrėnas, P., Baltrėnaitė, E., Šerevičienė, V., Pereira, P.: Atmospheric BTEX concentrations in the vicinity of the crude oil refinery of the Baltic region. Environ. Monit. Assess. **182**, 115–127 (2011)
3. Behrens, D.A., Koland, O., Leopold-Wildburger, U.: Why local air pollution is more than daily peaks: modelling policies in a city in order to avoid premature deaths. Cent. Eur. J. Oper. Res. **26**, 265–286 (2018)
4. Bolden, A.L., Kwiatkowski, C.F., Colborn, T.: New look at BTEX: are ambient levels a problem? Environ. Sci. Technol. **49**, 5261–5276 (2015)
5. Bose, S., Diette, G.B.: Health disparities related to environmental air quality. In: Health Disparities in Respiratory Medicine, pp. 41–58. Humana Press, Cham (2016)
6. Buczynska, A.J., Krata, A., Stranger, M., Godoi, A.F.L., Kontozova-Deutsch, V., Bencs, L., Naveau, I., Roekens, E., Van Grieken, R.: Atmospheric BTEX-concentrations in an area with intensive street traffic. Atmos. Environ. **43**, 311–318 (2009)
7. Burnett, R., Chen, H., Szyszkowicz, M., Fann, N., Hubbell, B., Pope, C.A., Apte, J.S., Brauer, M., Cohen, A., Weichenthal, S., Coggins, J.: Global estimates of mortality associated with long-term exposure to outdoor fine particulate matter. PNAS USA **115**, 9592–9597 (2018)
8. Campbell, P., Zhang, Y., Yan, F., Lu, Z., Streets, D.: Impacts of transportation sector emissions on future US air quality in a changing climate. Part II: Air quality projections and the interplay between emissions and climate change. Environ. Pollut. **238**, 918–930 (2018)
9. Carter, E., Archer-Nicholls, S., Ni, K., Lai, A.M., Niu, H., Secrest, M.H., Sauer, S.M., Schauer, J.J., Ezzati, M., Wiedinmyer, C., Yang, X.: Seasonal and diurnal air pollution from residential cooking and space heating in the Eastern Tibetan Plateau. Environ. Sci. Technol. **50**, 8353–8361 (2016)
10. Cerón Bretón, J.G., Cerón Bretón, R.M., Martínez Morales, S., Kahl, J.D., Guarnaccia, C., Lara Severino, R.D.C., Rangel Marrón, M., Ramírez Lara, E., Espinosa Fuentes, M.D.L.L., Uc Chi, M.P., Sánchez, G.L.: Health risk assessment of the levels of BTEX in ambient air of one

urban site located in Leon, Guanajuato, Mexico during two climatic seasons. Atmosphere **11**, 165 (2020)

11. Chen, T., Guestrin, C.: Xgboost: a scalable tree boosting system. In: Proceedings of the 22nd ACM SIGKDD International Conference on Knowledge Discovery and Data Mining, pp. 785–794 (2016)

12. Dehghani, M., Fazlzadeh, M., Sorooshian, A., Tabatabaee, H.R., Miri, M., Baghani, A.N., Delikhoon, M., Mahvi, A.H., Rashidi, M.: Characteristics and health effects of BTEX in a hot spot for urban pollution. Ecotoxicol. Environ. Saf. **155**, 133–143 (2018)

13. Fowler, D., Brimblecombe, P., Burrows, J., Heal, M.R., Grennfelt, P., Stevenson, D.S., Jowett, A., Nemitz, E., Coyle, M., Lui, X., Chang, Y.: A chronology of global air quality. Philos. Trans. R. Soc. A **378**, 20190314 (2020)

14. Gallego, E., Roca, F.X., Guardino, X., Rosell, M.G.: Indoor and outdoor BTX levels in Barcelona city metropolitan area and Catalan rural areas. J. Environ. Sci. **20**, 1063–1069 (2008)

15. García, M.V., Aznarte, J.L.: Shapley additive explanations for NO2 forecasting. Ecol. Inform. **56**, (2020)

16. Hajizadeh, Y., Mokhtari, M., Faraji, M., Mohammadi, A., Nemati, S., Ghanbari, R., Abdolah-nejad, A., Fard, R.F., Nikoonahad, A., Jafari, N., Miri, M.: Trends of BTEX in the central urban area of Iran: a preliminary study of photochemical ozone pollution and health risk assessment. Atmos. Pollut. Res. **9**, 220–229 (2018)

17. Holgate, S.T.: Every breath we take: the lifelong impact of air pollution-a call for action. Clin. Med. **17**, 8 (2017)

18. Kirman, C.R., Aylward, L.L., Blount, B.C., Pyatt, D.W., Hays, S.M.: Evaluation of NHANES biomonitoring data for volatile organic chemicals in blood: application of chemical-specific screening criteria. J. Expo. Sci. Environ. Epidemiol. **22**, 24–34 (2012)

19. Landrigan, P.J.: Air pollution and health. Lancet Public Health **2**, e4–e5 (2017)

20. Lerner, J.E.C., Kohajda, T., Aguilar, M.E., Massolo, L.A., Sánchez, E.Y., Porta, A.A., Opitz, P., Wichmann, G., Herbarth, O., Mueller, A.: Improvement of health risk factors after reduction of VOC concentrations in industrial and urban area. Environ. Sci. Pollut. Res. **21**, 9676–9688 (2014)

21. Lundberg S., Lee, S.: A unified approach to interpreting model predictions. In: Advances in Neural Information Processing Systems, pp. 4765–4774 (2017)

22. Liao, Z., Gao, M., Sun, J., Fan, S.: The impact of synoptic circulation on air quality and pollution-related human health in the Yangtze River Delta region. Sci. Total Environ. **607**, 838–846 (2017)

23. Liu, A., Hong, N., Zhu, P., Guan, Y.: Understanding benzene series (BTEX) pollutant load characteristics in the urban environment. Sci. Total Environ. **619**, 938–945 (2018)

24. Ly, H.B., Le, L.M., Phi, L.V., Phan, V.H., Tran, V.Q., Pham, B.T., Le, T.T., Derrible, S.: Development of an AI model to measure traffic air pollution from multisensor and weather data. Sensors **19**, 4941 (2019)

25. Marć, M., Namieśnik, J., Zabiegała, B.: BTEX concentration levels in urban air in the area of the Tri-City agglomeration (Gdansk, Gdynia, Sopot), Poland. Air Qual. Atmos. Health **7**, 489–504 (2014)

26. Milazzo, M.J., Gohlke, J.M., Gallagher, D.L., Scott, A.A., Zaitchik, B.F., Marr, L.C.: Potential for city parks to reduce exposure to BTEX in air. Environ. Sci. Process. Impacts **21**, 40–50 (2019)

27. Ning, G., Yim, S.H.L., Wang, S., Duan, B., Nie, C., Yang, X., Wang, J., Shang, K.: Synergistic effects of synoptic weather patterns and topography on air quality: a case of the Sichuan Basin of China. Clim. Dyn. **53**, 6729–6744 (2019)

28. Rattanajongjitrakorn, P., Prueksasit, T.: Temporal variation of BTEX at the area of petrol station in Bangkok, Thailand. APCBEE Procedia **10**, 37–41 (2014)

29. Słomińska, M., Konieczka, P., Namieśnik, J.: The fate of BTEX compounds in ambient air. Crit. Rev. Environ. Sci. Technol. **44**, 455–472 (2014)

30. Stingone, J.A., McVeigh, K.H., Claudio, L.: Early-life exposure to air pollution and greater use of academic support services in childhood: a population-based cohort study of urban children. Environ. Health **16**, 2 (2017)

31. Stojić, A., Stanić, N., Vuković, G., Stanišić, S., Perišić, M., Šoštarić, A., Lazić, L.: Explainable extreme gradient boosting tree-based prediction of toluene, ethylbenzene and xylene wet deposition. Sci. Total Environ. **653**, 140–147 (2019)
32. Stojić, A., Stojić, S.S., Mijić, Z., Šoštarić, A., Rajšić, S.: Spatio-temporal distribution of VOC emissions in urban area based on receptor modelling. Atmos. Environ. **106**, 71–79 (2015b)
33. Stojić, A., Stojić, S.S., Šoštarić, A., Ilić, L., Mijić, Z., Rajšić, S.: Characterization of VOC sources in urban area based on PTR-MS measurements and receptor modelling. Environ. Sci. Pollut. Res. **22**, 13137–13152 (2015a)
34. Stojić, A., Stojić, S.S.: The innovative concept of three-dimensional hybrid receptor modeling. Atmos. Environ. **164**, 216–223 (2017)
35. Šoštarić, A., Stojić, S.S., Vuković, G., Mijić, Z., Stojić, A., Gržetić, I.: Rainwater capacities for BTEX scavenging from ambient air. Atmos. Environ. **168**, 46–54 (2017)
36. Šoštarić, A., Stojić, A., Stojić, S.S., Gržetić, I.: Quantification and mechanisms of BTEX distribution between aqueous and gaseous phase in a dynamic system. Chemosphere **144**, 721–727 (2016)
37. Stanišić, S., Perišić, M., Jovanović, G., Milićević, T., Romanić, S.H., Jovanović, A., Šoštarić, A., Udovičić, V., Stojić, A.: The PM2.5-bound polycyclic aromatic hydrocarbon behavior in indoor and outdoor environments, Part I: emission sources. Environ. Res. 110520 (2020b)
38. Stanišić, S., Perišić, M., Stojić, A.: The use of innovative methodology for the characterization of benzene, toluene, ethylbenzene and xylene sources in the Belgrade area. In: Sinteza International Scientific Conference on Information Technology and Data Related Research, Belgrade, Serbia (2020a)
39. Truong, S.C., Lee, M.I., Kim, G., Kim, D., Park, J.H., Choi, S.D., Cho, G.H.: Accidental benzene release risk assessment in an urban area using an atmospheric dispersion model. Atmos. Environ. **144**, 146–159 (2016)
40. U.S. EPA.: Chemical Data Reporting. United States Environmental Protection Agency, Washington, DC, USA (2016). https://www.epa.gov/sites/production/files/2014-11/documents/2nd_cdr_snapshot_5_19_14.pdf
41. Vardoulakis, S., Solazzo, E., Lumbreras, J.: Intra-urban and street scale variability of BTEX, NO2 and O3 in Birmingham, UK: implications for exposure assessment. Atmos. Environ. **45**, 5069–5078 (2011)
42. Werder, E.J., Engel, L.S., Blair, A., Kwok, R.K., McGrath, J.A., Sandler, D.P.: Blood BTEX levels and neurologic symptoms in Gulf states residents. Environ. Res. **175**, 100–107 (2019)
43. Wright, C.Y., Millar, D.A.: A global statement for air pollution and health. Clean Air J. **29**, 1–2 (2019)

# Faraday and Resonant Waves in Dipolar Cigar-Shaped Bose-Einstein Condensates

Dušan Vudragović

Scientific Computing Laboratory, Center for the Study of Complex Systems,
*Institute of Physics Belgrade, University of Belgrade, Serbia*
e-mail:dusan@ipb.ac.rs

Faraday and resonant density waves emerge in Bose-Einstein condensates as a result of harmonic driving of the system [1-3]. They represent nonlinear excitations and are generated due to the interaction-induced coupling of collective oscillation modes and the existence of parametric resonances. Using a mean-field variational and a full numerical approach, we study density waves in dipolar condensates at zero temperature [1], where breaking of the symmetry due to anisotropy of the dipole-dipole interaction plays an important role. We derive variational equations of motion for the dynamics of a driven dipolar system and identify the most unstable modes that correspond to the Faraday and resonant waves. Based on this, we also derive the analytical expressions for spatial periods of both types of density waves as functions of the contact and the dipole-dipole interaction strength. Finally, we compare the obtained variational results with the results of extensive numerical simulations that solve the dipolar Gross-Pitaevskii equation in 3D.
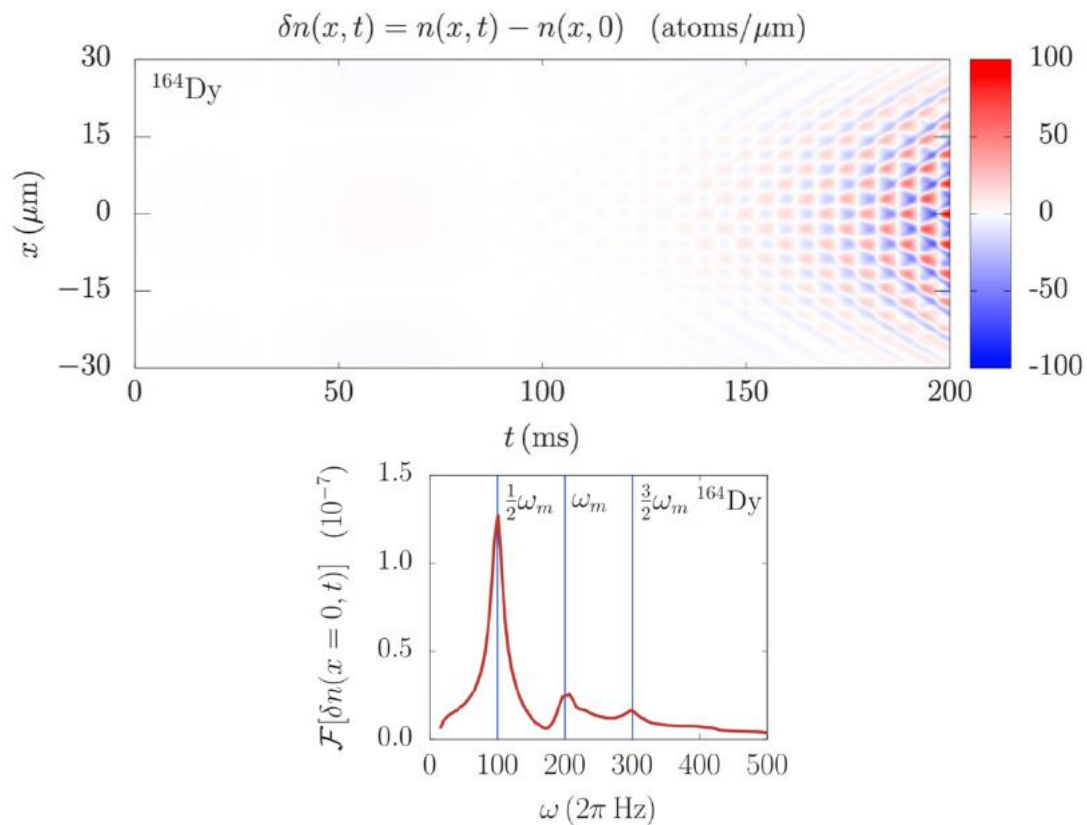
REFERENCES
[1] D. Vudragović and A. Balaž, Symmetry **11**, 1090 (2019).
[2] A. Balaž, R. Paun, A. I. Nicolin, et al., Phys. Rev. A **89**, 023609 (2014).
[3] A. Balaž and A. I. Nicolin, Phys. Rev. A **85**, 023613 (2012).
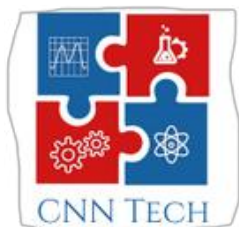
THE POTENTIAL FOR FORECASTING THE PARTICULATE MATTER LEVELS IN COMPLEX URBAN ENVIRONMENT

Mirjana Perisic [1,2], Andreja Stojic[1,2*], Gordana Jovanovic[1,2], Andrej Sostaric[3], Dimitrije Maletic[1], Dusan Vudragovic[1], Svetlana Stanisic[2]

[1]Institute of Physics Belgrade, National Institute of the Republic of Serbia, University of Belgrade, 118 Pregrevica Street, 11000, Belgrade, Serbia

[2]Singidunum University, 32 Danijelova Street, Belgrade, 11000, Serbia

[3]Institute of Public Health Belgrade, 54 Despota Stefana Street, 11000, Belgrade, Serbia

*Corresponding author e-mail: andreja.stojic@ipb.ac.rs

Abstract

In this study, we employed regression analysis by means of machine learning eXtreme Gradient Boosting method for estimating the relationships between particulate matter (PM_{10}) concentrations and a number of parameters including benzene, inorganic gaseous pollutants (SO_2, NO, NO_2, NOx), Global Data Assimilation System-modeled (GDAS1) meteorological parameters, as well as daily and weekend PM variations in Belgrade, Serbia. The data was provided by the Institute of Public Health Belgrade, Serbia. The successful and reliable predictions were provided with relative errors in the range from approx. 19% to 26% and correlation coefficients higher than 0.95. The lowest relative error and the highest correlation coefficient were obtained for monitoring station of rural/industrial type located in Ovca, while the highest difference between modeled and measured values were detected at urban-type monitoring stations Novi Beograd and Institute of Public Health Belgrade, both of which are exposed to traffic emissions. The modeling results were not satisfying for rural/industrial monitoring station located in Veliki Crljeni (relative error>30%, corr. coefficient<0,8), which implies that the dynamic of PM_{10} emissions at the selected monitoring site were not governed by the available data on pollutant concentrations and meteorological parameters.

Keywords

Particulate matter, air pollution forecast, machine learning

Acknowledgement

THE IMPACT OF GASEOUS POLLUTANTS ON PARTICULATE MATTER DISTRIBUTION

Svetlana Stanisic[2], Mirjana Perisic[1,2], Andreja Stojic[1,2*], Andrej Sostaric[3], Dusan Vudragovic[1], Dimitrije Maletic[1], Gordana Jovanovic[1,2]

[1]Institute of Physics Belgrade, National Institute of the Republic of Serbia, University of Belgrade, 118 Pregrevica Street, 11000, Belgrade, Serbia

[2]Singidunum University, 32 Danijelova Street, Belgrade, 11000, Serbia

[3]Institute of Public Health Belgrade, 54 Despota Stefana Street, 11000, Belgrade, Serbia

*Corresponding author e-mail: andreja.stojic@ipb.ac.rs

Abstract

In this study, we used eXtreme Gradient Boosting machine learning and SHapley Additive exPlanations (SHAP) explainable artificial intelligence methods to examine the relationships between PM_{10} and other air pollutant concentrations in the urban area of Belgrade. The data was provided by the Institute of Public Health Belgrade, Serbia. As shown, the most significant relative impact of benzene levels (50%) on the increase of PM_{10} concentrations up to several tens of μg m^{-3} was recorded at the occasions when benzene concentrations exceeded 5 μg m^{-3} and the concentrations of NO_2 were low (combustion of fossil fuels). The same effect was less pronounced at higher NO_2 concentrations. Taking into consideration the relative impact of SO_2 on PM_{10} levels and the observed relationship between NO and PM_{10}, four dominant environment types that describe the PM level dynamics were distinguished. In the first-type environment, the decrease of PM_{10} levels noticed for SO_2 levels below 50 μg m^{-3} and the dominance of sources with a significant share of NO (> 120 μg m^{-3}) were attributed to traffic emissions. The ambiance recognized as type 2 with no effect on PM levels is characterized by low gaseous oxide concentrations. The third and the fourth type of environment are characterized by SO_2 values exceeding 50 μg m^{-3} and their significant impact on the increase of PM_{10} concentrations.

Keywords

particulate matter, inorganic gaseous pollutants, explainable artificial intelligence

Acknowledgement

SPATIO-TEMPORAL ANALYSIS OF MOBILITY PATTERNS IN THE CITY OF BELGRADE

Nikola Stupar[1], Ana Vranic[1], Andreja Stojic[1,2], Gordana Vukovic[1,2], Dusan Vudragovic[1], Dimitrije Maletic[1], Marija Mitrovic Dankulov[1*]

[1] Institute of Physics Belgrade, University of Belgrade, Pregrevica 118, 11080 Belgrade, Serbia

[2] Singidunum University, 32 Danijelova Street, Belgrade, 11000, Serbia

Corresponding author e-mail: mitrovic@ipb.ac.rs

Abstract

Information about human mobility is essential for sustainable development planning. It is crucial for urban and transportation planning and the role of mobility in reducing contributions of human activities in air pollution and fighting climate change. While *human* mobility patterns are typically stable over space and time, they can dramatically change due to critical events, such as earthquakes and epidemics. We still lack a detailed description and understanding of how these critical events influence mobility patterns. In this work, we combine artificial intelligence tools with tools and methods from complex network theory to study human mobility patterns in the City of Belgrade during the COVID-19. We use data about mobility in the City of Belgrade between May 2020 and January 2021 from the Facebook Data for Good dataset. The City of Belgrade is divided into 201 cells with information on the mobility before and during the crises within and between the cells. The time resolution of the data is 8 hours. We use the k-mean clustering technique to cluster the data and find five clusters with different average mobility patterns. All mobility time series have trends and cycles, but they differ between clusters. While residential and suburban area clusters have the peaks of activity during the working days, clusters including central municipalities have the peak of activity during Saturday afternoon. Our results show that different city areas react differently to COVID19 information and that this aspect has to be considered in air pollution and crisis management planning.

Keywords

mobility patterns, time series analysis, k-means clustering

Acknowledgement

Faraday and Resonant Waves in Dipolar Cigar-Shaped Bose-Einstein Condensates

D. Vudragović and A. Balaž

Institute of Physics Belgrade, University of Belgrade, Serbia

Faraday and resonant density waves emerge in Bose-Einstein condensates as a result of harmonic driving of the system [1-3]. They represent nonlinear excitations and are generated due to the interaction-induced coupling of collective oscillation modes and the existence of parametric resonances. Using a mean-field variational and a full numerical approach, we study density waves in dipolar condensates at zero temperature [1], where breaking of the symmetry due to anisotropy of the dipole-dipole interaction (DDI) plays an important role. We derive variational equations of motion for the dynamics of a driven dipolar system and identify the most unstable modes that correspond to the Faraday and resonant waves. Based on this, we also derive the analytical expressions for spatial periods of both types of density waves as functions of the contact and the DDI strength. Finally, we compare the obtained variational results with the results of extensive numerical simulations that solve the dipolar Gross-Pitaevskii equation in 3D.
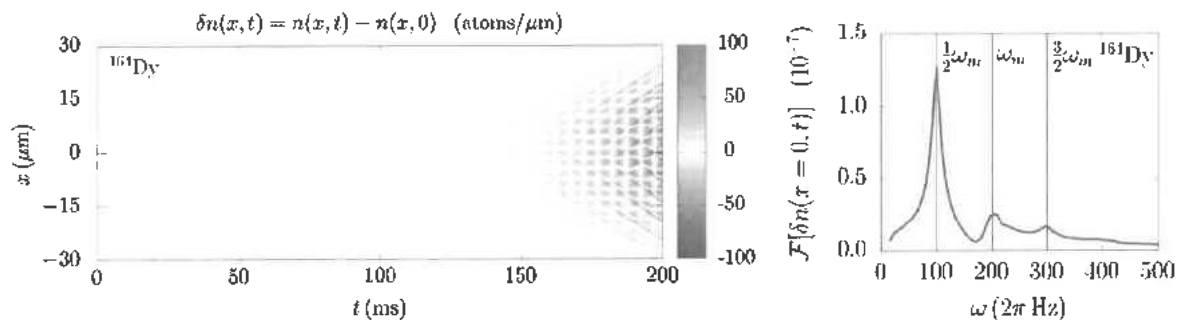
References

[1] D. Vudragović and A. Balaž, Symmetry **11**, 1090 (2019).

[2] A. Balaž, R. Paun, A. I. Nicolin, et al., Phys. Rev. A **89**, 023609 (2014).

[3] A. Balaž and A. I. Nicolin, Phys. Rev. A **85**, 023613 (2012).

Подаци о цитираности

Следећи подаци о цитираности др Душана Вудраговића извезени су из Web of Science платформе дана 15. октобра 2024. године.

Publications

11
Total

From 1996 ⌄ to 2024 ⌄

Citing Articles

296 Analyze
Total

292 Analyze
Without self-citations

Times Cited

402
Total

36.55
Average per item

393
Without self-citations

7
H-Index

Times Cited and Publications Over Time
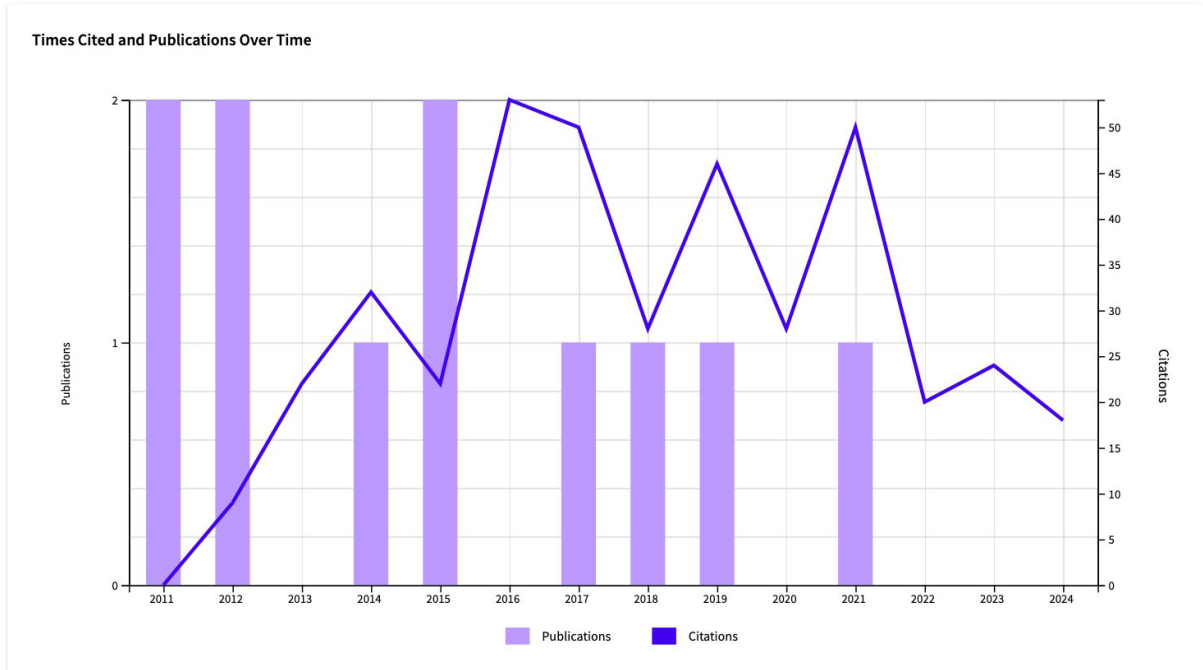
11 Publications	Citations: highest first ▾	<	1 of 1	>	Citations						
					‹ Previous year			Next year ›		Average per year	Total
					2020	2021	2022	2023	2024		
				Total	28	50	20	24	18	30.92	402
⊖ 1	C programs for solving the time-dependent Gross-Pitaevskii equation in a fully anisotropic trap Vudragovic, D; Vidanovic, I; (...); Adhikari, SK Sep 2012	COMPUTER PHYSICS COMMUNICATIONS ▾ 183 (9) , pp.2021-2025				13	16	4	6	5	14.31	186
⊖ 2	Fortran and C programs for the time-dependent dipolar Gross-Pitaevskii equation in an anisotropic trap Kumar, RK; Young, LE; (...); Adhikari, SK Oct 2015	COMPUTER PHYSICS COMMUNICATIONS ▾ 195 , pp.117-128				7	11	9	5	7	10.7	107
⊖ 3	OpenMP GNU and Intel Fortran programs for solving the time-dependent Gross-Pitaevskii equation Young, LE; Muruganandam, P; (...); Balaz, A Nov 2017	COMPUTER PHYSICS COMMUNICATIONS ▾ 220 , pp.503-506				5	6	2	3	1	4	32

⊖ 4	**Spin-1 spin-orbit- and Rabi-coupled Bose-Einstein condensate solver** Ravisankar, R; Vudragovic, D; (...); Adhikari, SK Feb 2021 | COMPUTER PHYSICS COMMUNICATIONS ▾ 259	0	12	5	6	1	6	24
⊖ 5	**Development of Grid e-Infrastructure in South-Eastern Europe** Balaz, A; Prnjat, O; (...); Savic, M Jun 2011 | JOURNAL OF GRID COMPUTING ▾ 9 (2) , pp.135-154	0	0	0	0	0	1.64	23
⊖ 6	**Development of collisional data base for elementary processes of electron scattering by atoms and molecules** Marinkovic, BP; Vujcic, V; (...); Mason, NJ Jul 1 2015 | NUCLEAR INSTRUMENTS & METHODS IN PHYSICS RESEARCH SECTION B-BEAM INTERACTIONS WITH MATERIALS AND ATOMS ▾ 354 , pp.90-95	2	2	0	1	1	1.3	13
⊖ 7	**Faraday and Resonant Waves in Dipolar Cigar-Shaped Bose-Einstein Condensates** Vudragovic, D and Balaz, A Sep 2019 | SYMMETRY-BASEL ▾ 11 (9)	1	2	0	3	2	1.33	8
⊖ 8	**SPEEDUP Code for Calculation of Transition Amplitudes via the Effective Action Approach** Balaz, A; Vidanovic, I; (...); Bogojevic, A Mar 2012 | COMMUNICATIONS IN COMPUTATIONAL PHYSICS ▾ 11 (3) , pp.739-755	0	0	0	0	0	0.46	6
⊖ 9	**SEE-GRID eInfrastructure for Regional eScience** Prnjat, O; Balaz, A; (...); Neagu, G International Symposium on Grid Computing 2011 | DATA DRIVEN E-SCIENCE, ISGC 2010 , pp.91-103	0	0	0	0	1	0.14	2
⊖ 10	**Implementation and Benchmarking of New FFT Libraries in Quantum ESPRESSO** Stankovic, D; Jovanovic, P; (...); Balaz, A HP-SEE User Forum 2014 | HIGH-PERFORMANCE COMPUTING INFRASTRUCTURE FOR SOUTH EAST EUROPE'S RESEARCH COMMUNITIES: RESULTS OF THE HP-SEE USER FORUM 2012 2 , pp.155-162	0	1	0	0	0	0.09	1
⊖ 11	**VI-SEEM DREAMCLIMATE SERVICE** Vudragovic, D; Ilic, L; (...); Balaz, A Jun 2018 | SCALABLE COMPUTING-PRACTICE AND EXPERIENCE ▾ 19 (2) , pp.215-221	0	0	0	0	0	0	0

Република Србија
**МИНИСТАРСТВО ПРОСВЕТЕ,
НАУКЕ И ТЕХНОЛОШКОГ РАЗВОЈА**
Матични научни одбор за физику

Број: 660-01-4/2020-14/18
22.05.2020. године
Б е о г р а д

На основу члана 27. став 1 тачка 1) и члана 76. став 5. Закона о науци и истраживањима („Службени гласник Републике Србије", бр. 49/2019) и Правилника о поступку, начину вредновања и квантитативном исказивању научноистраживачких резултата истраживача („Службени гласник Републике Србије", број 24/16, 21/17 и 38/17) и захтева који је поднео

Институт за физику у Београду

Матични научни одбор за физику на седници одржаној 22.05.2020. године, донео је

ОДЛУКУ
О СТИЦАЊУ НАУЧНОГ ЗВАЊА

Др Душан Вудраговић

стиче научно звање
Научни сарадник

у области природно-математичких наука - физика

О Б Р А З Л О Ж Е Њ Е

Институт за физику у Београду

утврдио је предлог број 0801-441/1 од 12.05.2020. године на седници Научног већа Института за физику у Београду и поднео захтев Матичном научном одбору за физику број 0801-441/2 од 12.05.2020. године за доношење одлуке о испуњености услова за стицање научног звања **Научни сарадник.**

Матични научни одбор за физику на седници одржаној 22.05.2020. године разматрао је захтев и утврдио да именовани испуњава услове из члана 76. став 5. Закона о науци и истраживањима („Службени гласник Републике Србије", бр. 49/2019) и Правилника о поступку, начину вредновања и квантитативном исказивању научноистраживачких резултата истраживача („Службени гласник Републике Србије", број 24/16, 21/17 и 38/17) за стицање научног звања **Научни сарадник** па је одлучио као у изреци ове одлуке.

Доношењем ове одлуке именовани стиче сва права која му на основу ње по закону припадају.

Одлуку доставити подносиоцу захтева, именованом и архиви Министарства просвете, науке и технолошког развоја у Београду.

МИНИСТАР

Младен Шарчевић

**МАТИЧНИ НАУЧНИ ОДБОР ЗА ФИЗИКУ
ПРЕДСЕДНИК**

проф. др Милан Дамњановић

Рецензије научних радова

ScholarOne Manuscripts™

Dusan Vudragovic ▾ | Instructions & Forms | Help | Log Out

emerald PUBLISHING

Data Technologies & Applications

⌂ Home | ✎ Author | 💬 Review

Referee View Manuscripts

Referee View Manuscripts

0 Review and Score ›
5 Scores Submitted ›
4 Receive Recognition on Web of Science ›
Invitations ›

Scores Submitted

ACTION	COMPLETED	ID/TITLE	STATUS
Select...	11-Oct-2021	DTA-08-2021-0193 Dynamic Distributed and Flexible Machine Learning Algorithms for Big Data Mining Processing Files archived ⊞	Accept (23-Nov-2021) *Archiving completed on 27-Dec-2021* Assignments: AE: Ivanov, Todor EIC: Miguel Ángel, Sicilia Urbán GE: Not Assigned
Select...	23-Apr-2019	DTA-11-2018-0087-R1 Hadoop-based Experimental Evaluation of MapReduce Designed HMeans for Distributed Document Clustering Files archived ⊞	Reject (01-May-2019) *Archiving completed on 21-Oct-2019* Assignments: AE: Ivanov, Todor EIC: Miguel Ángel, Sicilia Urbán GE: Not Assigned
Select...	29-Jan-2019	DTA-12-2018-0108 Identification of operational demand in law enforcement agencies: an application based on a probabilistic model of topics	Major Revision (11-Feb-2019) a revision has been submitted Assignments: AE: Not Assigned EIC: Miguel Ángel, Sicilia Urbán GE: Lytras, Miltiadis
Select...	12-Sep-2018	DTA-06-2018-0034 A Framework for Multi-Resource Fair Allocation Based on TS-HF Allocation Mechanism and Scheduling using VMs in Cloud Computing Files archived ⊞	Reject (30-Sep-2018) *Archiving completed on 01-Feb-2019* Assignments: AE: Sartori, Fabio EIC: Miguel Ángel, Sicilia Urbán GE: Not Assigned
Select...	10-Jul-2018	DTA-05-2018-0040 Parallelization and Analysis of Numerical Algorithms on Shared Memory Architecture	Major Revision (17-Sep-2018) a revision has been submitted Assignments: AE: Miguel Ángel, Sicilia Urbán EIC: Miguel Ángel, Sicilia Urbán GE: Not Assigned

home | main menu | submit paper | guide for authors | register | change details | log out

Contact us ✉
Help ?

Username: dusan.vudragovic@ipb.ac.rs
Switch To: Reviewer ▼   Go to: My EES Hub

Version: EES 2020.2

PHYSICS LETTERS A

Completed Reviewer Assignments for Dušan Vudragovic

Page: 1 of 1 (2 total assignments)

Display 10 ▼ results per page.

Action	My Reviewer Number ▲▼	Manuscript Number ▲▼	Article Type ▲▼	Article Title ▲▼	Date Reviewer Invited ▲▼	Date Reviewer Agreed ▲▼	Date Review Due ▲▼	Date Review Submitted ▲▼	Days Taken ▲▼	Editor's Name ▲▼	Corr. Author ▲▼
Action Links	2		Letter		Sep 28, 2018	Oct 05, 2018	Oct 19, 2018	Oct 16, 2018	18		
Action Links	2		Letter		Jul 08, 2018	Jul 09, 2018	Jul 30, 2018	Aug 07, 2018	30		

Page: 1 of 1 (2 total assignments)

Display 10 ▼ results per page.

<< Reviewer Main Menu

You should use the free Adobe Acrobat Reader 6 or later for best PDF Viewing results.

Get Adobe Acrobat Reader

em | SPRINGER NATURE **Applied Physics B**

Home | Main Menu | Submit a Manuscript | About ⌄ | Help ⌄

← **Completed Reviewer Assignments**

Page: 1 of 1 (2 total assignments)

Results per page 10 ⌄

Action	My Reviewer Number	Manuscript Number	Article Type	Article Title	Current Status	Final Disposition	Date Reviewer Invited	Date Reviewer Agreed	Date Review Due	Date Review Submitted ▸	Days Taken	Editor's Name	Corr. Author
Action Links	3		Regular Paper		Completed Accept	Accept	09 May 2021	10 May 2021	28 May 2021	31 May 2021	21		
Action Links	3		Regular Paper		Completed Accept	Accept	18 Mar 2021	19 Mar 2021	09 Apr 2021	14 Apr 2021	26		

Page: 1 of 1 (2 total assignments)

Results per page 10 ⌄

IOP | Journal of Physics: Condensed Matter

now required
for submission

🏠 Home   ✎ Author   💬 Review

Referee View Manuscripts

Referee View Manuscripts

0 Review and Report >

1 Reports Submitted >

   Invitations >

Reports Submitted

WANT TO BE A MORE CONFIDENT REVIEWER?
TAKE OUR FREE ONLINE COURSE TODAY.
CLICK HERE TO GET STARTED.

ACTION	COMPLETED	ID/TITLE	STATUS
Select...	15-Oct-2023	JPCM-123394 Effect of Zero-Point Motion on Properties of Quantum Particles adsorbed on a Substrate Files archived 🗎	Moderate Revision (16-Nov-2023) a revision has been submitted *Archiving completed on 05-Apr-2024*

SIMULATION
Transactions of The Society for Modeling and Simulation International

Sage Track

☰ Home | **✎ Author** | **💬 Review**

Referee View Manuscripts

Referee View Manuscripts

0	Review and Score >
1	Scores Submitted >
1	Receive Recognition on Web of Science >
	Invitations >

Submitted Reviews Available for Credit

INCLUDE	COMPLETED	ID/TITLE	STATUS
☐	24-Dec-2019	A-19-0220 Efficient aerodynamic shape optimization through reduced order CFD modeling Files archived 🔒	Reject (30-Mar-2020) *Archiving completed on 31-Mar-2021*

Select All >   **Receive Recognition >**

The

EOSC Regional Event

by **NI4OS** Europe

Embedding **EOSC** *in Southeast Europe*

SEPTEMBER 28-29, 2022
BUDAPEST UNIVERSITY OF TECHNOLOGY AND ECONOMICS

DAY 1

Room 1

9:00	Registration

10:00 *Open Science Cloud in the Southeast European region and beyond*

Chair:
Prof. Anastas Mishev

Open Science challenges and success in Hungary
– *Dr. István Szabó, Vice President of the National Research, Development and Innovation Office*
2 decades of South-East European regional cooperation
– *Dr. Ognjen Prnjat, NI4OS-Europe coordinator; Director of European Infrastructures and Projects, National Infrastructures for Research and Technology (GRNET)*
EOSC Association: technical vision
– *Rene Buch, Chief Technical Officer, EOSC Association*
EOSC as part of the EC strategy for Open Science
– *Dr. Michel Schouppe, Senior expert and team leader on EOSC, Open Science Unit, DG R&I*

11:30	Coffee Break

11:50 *Pan-European Cloud: global coverage*

Chair:
Dr. Michel Schouppe

EOSC-Nordic and its regional impact
– *Dr. Lene Krøl Andersen, International Liaison, Computerome*
EOSC-Pillar
– *Jos van Wezel, International Projects Coordinator, KIT, Germany*
EOSC-Synergy
– *Viet Tran, PhD., Senior researcher, Institute of Informatics, Slovak Academy of Sciences*
Panel, including NI4OS-Europe
– *Eleni Toli, Project Director, NI4OS-Europe; Researcher, ATHENA*

13:20	Lunch

14:20 *Capacity provisioning for EOSC*

Chair:
Eleni Toli

Data services and DICE project
– *Dr. Debora Testi, DICE project coordinator, EUDAT user engagement leader, CINECA*
Computing services and EGI-ACE project
– *Dr. Gergely Sipos, Head of Services, Solutions and Support, EGI Foundation*
Open publishing services and OpenAIRE-Nexus project
– *Natalia Manola, CEO, OpenAIRE*
C-SCALE: Enabling Copernicus Big Data Analytics through EOSC
– *Dr. Christian Briese, Managing Director, EODC*

15:50	Coffee Break

16:10 *EOSC-Future and the ecosystem*

Chair:
Prof. Aneta Karaivanova

EOSC-Future platform: focus on Western Balkans
– *Dr. Anastas Mishev, Professor, Ss. Cyril and Methodius University in Skopje*
EOSC Working Groups
– *Dr. Ilias Papastamatiou, Senior Project Manager, GRNET*
Integrated training platforms and skills
– *Dr. Sonja Filiposka, Professor, Ss. Cyril and Methodius University in Skopje*
EOSC Promoters in NI4OS-Europe
– *Vasiliki Koukounidou, University Officer, University of Cyprus Library*

DAY 1

Room 2

9:00	Registration

11:30	Coffee Break

Life Sciences

**Chair:
Dr. Zoe Cournia**

11:50 — **Life Sciences in NI4OS-Europe and the region**
– *Dr. Zoe Cournia, Senior Researcher, Biomedical Research Foundation, Academy of Athens*

12:05 — **HPC for germline variant calling pipeline for human whole genome data**
– *Dr. Mirjana Novkovic, Assistant Research Professor, Institute of Molecular Genetics and Genetic Engineering, University of Belgrade*

12:20 — **Targeting protein-membrane interfaces using NI4OS-Europe resources**
– *Dr. Alexios Chatzigoulas, Postdoctoral Researcher, Biomedical Research Foundation of the Academy of Athens*

12:35 — **Cloud platform for discovery of targeted drug delivery systems**
– *Elena Kusevska, FCSE, Ss. Cyril and Methodious University in Skopje*

12:50 — **EEGHUB.GE: Brain electrical activity**
– *Dr. Irma Khachidze, Scientist, I. Beritashvili Center of Experimental Biomedicine, Tbilisi, Georgia*

13:20	Lunch

Climate & Meteorology

**Chair:
Dr. Theo Christoudias**

14:20 — **Climate Science in NI4OS-Europe and the region**
– *Dr. Theo Christoudias, Associate Professor, The Cyprus Institute*

14:35 — **Reduced precision chemical kinetics in atmospheric models**
– *Kyriakos Sofokleous, PhD Student, The Cyprus Institute*

14:50 — **Airquality prediction service**
– *Dr. Boro Jakimovski, Professor, Dean of FCSE, Ss. Cyril and Methodious University in Skopje*

15:05 — **Computational climate science and systems in Armenia**
– *Dr. Hrachya Astsatryan, Head of Scientific Computing Center, National Academy of Sciences of Armenia, Yerevan*

15:20 — **Remote sensing scene classification**
– *Dr. Vladimir Risojevic, Associate Professor, Faculty of Electrical Engineering, University of Banja Luka*

15:50	Coffee Break

Digital Cultural Heritage

**Chair:
Dr. George Artopoulos**

16:10 — **DCH in NI4OS-Europe and the region**
– *Dr. George Artopoulos, Associate Professor, The Cyprus Institute*

16:55 — **Platform for Digitization of Old and Heterogeneous Documents**
– *Drd. Tudor Bumbu, Vladimir Andrunachievici Institute of Mathematics and Computer Science*

16:25 — **2D color matching of fresco fragments with HPC**
– *Dr. Sofia Ivanovska, Associate Professor, Institute of Information and Communication Technologies, Bulgarian Academy of Sciences*

16:40 — **CHERE - Cultural Heritage Repository**
– *Dr. Mihajlo Savic, Professor, Faculty of Electrical Engineering, University of Banja Luka*

17:10 — **A user-driven content management system for DCH: C4DCH**
– *Maria Tzima, Software Developer for Data Management, The Cyprus Institute*

DAY 2

Room 1

| 8:30 | Registration |

9:00 *Policy aspects of EOSC*

Chair:
Dr. Srna Sudar

Status of National Open Science Cloud Initiatives in SEE
– *Eleni Toli, Project Director, NI4OS-Europe; Researcher, ATHENA*
EOSC MAR and SRIA
– *René Buch, Chief Technical Officer, EOSC Association*
Mandated organisation case study: KIFÜ, Hungary
– *János Mohácsi, International R&D Officer, Governmental Information-Technology Development Agency (KIFÜ)*
NOSCI case study: Bulgaria
– *Dr. Aneta Karaivanova, Professor, Scientific Secretary, IICT-BAS*
Joint Q&A

| 10:30 | Coffee Break |

10:50 *Generic services in Southeast European region*

Chair:
Prof. Boro Jakimovski

NI4OS-Europe catalogue and generic services
– *Dr. Dusan Vudragovic, Assistant Research Professor, Institute of Physics Belgrade*
Hungarian HPC offering and future plans
– *Dr. Tamás Máray, Head of HPC Competence Center, Governmental Information-Technology Development Agency (KIFÜ)*
DAEDALUS: upcoming HPC regional collaboration
– *Dr. Evangelia Athanasaki, Deputy Director, European Infrastructures and Projects, National Infrastructures for Research and Technology (GRNET)*

| 12:20 | Lunch |

13:20 *NI4OS-Europe tools for service providers*

Chair:
Dr. Dusan Vudragovic

Pre-production environment and service onboarding
– *Prof. Dr. Anastas Mishev, Professor, Ss. Cyril and Methodius University in Skopje*
NI4OS-Europe core services
– *Themis Zamani, Head of Implementation Unit, European Infrastructures and Projects Directorate, GRNET*
Repository onboarding
– *Milica Ševkušić, Librarian, Serbian Academy of Sciences and Arts*

| 14:50 | Coffee Break |

15:10 *Closing session*

Chair:
Dr. Ognjen Prnjat

Open Science Cloud: Users' vision
– *Dr. Ljupco Pejov, Professor, Ss. Cyril and Methodius University in Skopje*
– *Dr. Zoe Cournia, Senior Researcher, Biomedical Research Foundation, Academy of Athens*

DAY 2	8:30	Registration
Room 2		*Computational Physics*

9:00	**Computational physics in NI4OS-Europe and the region**
	– *Dr. Bojana Koteska, Assistant Professor, Ss. Cyril and Methodius University in Skopje*
9:15	**A more exact interpretation of IRMPD spectroscopic data analysis**
	– *Blagoj Achevski, Research Assistant, Faculty of Pharmacy,*
	Ss. Cyril and Methodius University in Skopje
9:45	**Engineering pharmaceutical crystals**
	– *Dejan Kuneski, Researcher, Department of Research and Technological Development, ALKALOID AD SKOPJE*
10:00	**Study of magnetic properties of nanoclusters**
	– *Dr. Yurii Chumakov, Leading Scientific Researcher, Institute of Applied Physics of Moldova*
10:15	**Transport in strongly interacting electron-phonon systems**
	– *Dr. Veljko Jankovic, Assistant Research Professor, Institute of Physics Belgrade*
10:30	**Properties of the square-lattice Hubbard model**
	– *Dr. Sonja Predin, Assistant Research Professor, Institute of Physics Belgrade*

**Chair:
Dr. Bojana Koteska**

10:45	Coffee Break

11:05	*Open Research Data Management tools*
	Tools for researchers and support to policies
	– *Dr. Branko Marović, Deputy director, RCUB, University of Belgrade*
	License clearance tool
	– *Panagiota Koltsida, Research Associate, ATHENA*
	EOSC RoP Legal and ethics compliance with RoLECT
	– *Eleni Toli, Project Director, NI4OS-Europe; Researcher, ATHENA*

**Chair:
Milica Ševkušić**

12:35	Lunch

	Other/Inter-disciplinary Services
13:35	**Audio-video-based vehicle detection and speed estimation**
	– *Dr. Slobodan Djukanovic, Faculty of Electrical Engineering, University of Montenegro*
13:50	**Sandpaper: exporting edge computing to EOSC**
	– *Dr. Katja Gilly, Associate Professor, Miguel Hernández University*
14:05	**Open access web application for metric skeletal sex estimation**
	– *Dr. Chrysovalantis Constantinou, Computational Scientist, The Cyprus Institute*
14:20	**Cloud service for automatic image mosaicking and georeferencing**
	– *Dr. Milutin Radonjić, Associate Professor, Faculty of Electrical Engineering, University of Montenegro*
14:35	**Phase transition recognition using deep learning autoencoders**
	– *Dr. Srijit Paul, Postdoctoral Researcher, University of Edinburgh*

**Chair:
Dr. Andreas Athenodorou**

14:50	Coffee Break

HP-SEE User Forum 2012 Committees

Programme Committee Chairs

Mihnea Dulea, IFIN-HH, Romania

Aneta Karaivanova, IICT-BAS, Bulgaria

Panayiota Poirazi, GRNET, Greece

Ognjen Prnjat, GRNET, Greece

Programme Committee Members

Aleksandar Belic, IPB, Serbia

Alexandru Nicolin, IFIN-HH, Romania

Anastas Misev, UKIM, Macedonia

Antun Balaz, IPB, Serbia

Emanouil Atanassov, IICT-BAS, Bulgaria

Hrachya Astsatryan, IIAP NAS RA, Armenia

Ioannis Liabotis, GRNET, Greece

Klaus Klingmueller, CASTORC, Cyprus

Manthos G. Papadopoulos, IOPC, Greece

Miklos Kozlovszky, SZTAKI, Hungary

Neki Frasheri, PUoT, Albania

Nenad Vukmirovic, IPB, Serbia

Peter Stefan, NIIF, Hungary

Petru Bogatencov, RENAM, Moldova

Ramaz Kvatadze, GRENA, Georgia

Organization Committee

Danica Stojiljkovic, IPB, Serbia

Aleksandar Belic, IPB, Serbia

Antun Balaz, IPB, Serbia

Dusan Vudragovic, IPB, Serbia

Vladimir Slavnic, IPB, Serbia

Ioannis Liabotis, GRNET, Greece

Ognjen Prnjat, GRNET, Greece

Dimitra Kotsokali, GRNET, Greece

Nikola Grkic, IPB, Serbia

Milica Cvetkovic, IPB, Serbia

Мнистарство науке, технолошког развоја и иновација
Матични научни одбор за геонауке и астрономију
Датум: 22.10.2024. године
Београд

Институт за физику у Београду
др Душан Вудраговић

11080 Београд
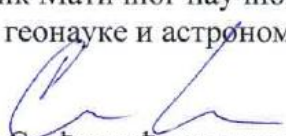Прегревица 118

Поштовани др Вудраговићу,

Матични научни одбор за геонауке и астрономију је на својој седници од 22. октобра 2024. године, разматрао Ваш захтев за признавање и категорисање публикације:

- Stanišić, S., Perišić, M., Jovanović, G., Maletić, D., Vudragović, D., Vranić, A. & Stojić, A. (2021) What Information on Volatile Organic Compounds Can Be Obtained from the Data of a Single Measurement Site Through the Use of Artificial Intelligence? In: Pap, E. (ed) Artificial Intelligence: Theory and Applications. Studies in Computational Intelligence, vol 973, 207–225. Springer, Cham. https://doi.org/10.1007/978-3-030-72711-6_12.

Одбор је једногласно донео одлуку да се наведена публикација категорише као резултат из категорије **M13** (монографска студија/поглавље у књизи M11 или рад у тематском зборнику водећег међународног значаја) у складу са Правилником о стицању истраживачких и научних звања.

С поштовањем,

Председник Матичног научног одбора
за геонауке и астрономију

др Владимир Срећковић, научни саветник